


ARTICLE

# Functional interactions between Mi-2 $\beta$ and AP1 complexes control response and recovery from skin barrier disruption

Sayaka Shibata, Mariko Kashiwagi, Bruce A. Morgan, and Katia Georgopoulos 

**Keratinocytes respond to environmental signals by eliciting induction of genes that preserve skin’s integrity. Here we show that the transcriptional response to stress signaling is supported by short-lived epigenetic changes. Comparison of chromatin accessibility and transcriptional changes induced by barrier disruption or by loss of the nucleosome remodeler Mi-2 $\beta$  identified their striking convergence in mouse and human keratinocytes. Mi-2 $\beta$  directly repressed genes induced by barrier disruption by restricting AP1-enriched promoter-distal sites, occupied by Mi-2 $\beta$  and JUNB at steady state and by c-JUN after Mi-2 $\beta$  depletion or stress signaling. Barrier disruption led to a modest reduction in Mi-2 $\beta$  expression and a further selective reduction of Mi-2 $\beta$  localization at stress response genes, possibly through competition with activated c-JUN. Consistent with a repressive role at stress response genes, genetic ablation of Mi-2 $\beta$  did not prevent reestablishment of barrier integrity but was required for return to homeostasis. Thus, a competition between Mi-2 $\beta$ -repressive and activating AP1 complexes may permit rapid transcriptional response to and resolution from stress signaling.**

## Introduction

Skin represents the largest interface of a living organism with the outer world and provides both a physical and immunological barrier against incoming threats, including mechanical injury, chemical insults, invading pathogens, and UV exposure (Segre, 2006). These environmental cues elicit stress signaling in keratinocytes that causes their activation and alters interactions with neighboring cells, including those of the immune system (Dainichi et al., 2018; Nestle et al., 2009; Pittelkow, 2005). Swift recovery from a stress response is also important for return to skin homeostasis, with sustained stress signaling contributing to pathogenic conditions that are often characterized by excess inflammation and epidermal barrier dysfunction (Dainichi et al., 2018; Nestle et al., 2009; Pittelkow, 2005).

During keratinocyte differentiation, a large number of genes are in a poised chromatin state with some pre-established interactions reported between promoters and enhancers (Rubin et al., 2017). In addition to transcriptional activators, chromatin modifiers play an important role in providing a poised chromatin landscape. Mi-2 $\beta$  is an ATP-dependent nucleosome remodeler that serves as a core component of the nucleosome remodeling and deacetylase (NuRD) complex (Tong et al., 1998; Xue et al., 1998; Zhang et al., 1998). Two types of enzymes in the

NuRD complex, the histone deacetylases (HDACs) HDAC1 and HDAC2 and the nucleosome remodeler Mi-2 $\beta$ , work together to modulate transcription. By altering nucleosome position relative to transcription factor (TF) binding sites (Becker, 2002; Brehm et al., 2000), Mi-2 $\beta$  can either promote or suppress gene expression depending on local context (Williams et al., 2004; Yoshida et al., 2008; Zhang et al., 2011). Mi-2 $\beta$  is expressed in many progenitor cell types, including embryonic stem cells, hematopoietic cells and neuronal, epithelial, and heart muscle precursors where it is required to keep genes supporting alternate cell fates in a poised but repressed state and prevent precocious differentiation (Gómez-Del Arco et al., 2016; Kim et al., 1999; Reynolds et al., 2012; Yamada et al., 2014; Yoshida et al., 2008; Yoshida et al., 2019; Zhang et al., 2011).

During embryonic and fetal development of the epidermis, NuRD complex components regulate cell fate choices by engaging in stage-specific transcriptional networks that control epidermal differentiation (Kashiwagi et al., 2007; LeBoeuf et al., 2010). HDAC1/2 are required for the differentiation of basal epidermal cells into suprabasal and follicular cell fates by providing repressive function to p63, an early epidermal differentiation factor, and for keratinocyte proliferation by inhibiting

.....  
 Cutaneous Biology Research Center, Massachusetts General Hospital, Harvard Medical School, Charlestown, MA.

Correspondence to Katia Georgopoulos: [katia.georgopoulos@cbrc2.mgh.harvard.edu](mailto:katia.georgopoulos@cbrc2.mgh.harvard.edu); Sayaka Shibata: [sshibata1@mgh.harvard.edu](mailto:sshibata1@mgh.harvard.edu).

© 2019 Shibata et al. This article is distributed under the terms of an Attribution–Noncommercial–Share Alike–No Mirror Sites license for the first six months after the publication date (see <http://www.rupress.org/terms/>). After six months it is available under a Creative Commons License (Attribution–Noncommercial–Share Alike 4.0 International license, as described at <https://creativecommons.org/licenses/by-nc-sa/4.0/>).

p53 activity through deacetylation (LeBoeuf et al., 2010; Luo et al., 2000). Mi-2 $\beta$  is required for commitment of the embryonic ectoderm to the epidermal cell lineage as well for self-renewal of the newly generated epidermal precursors; however, it is not required for their stratification (Kashiwagi et al., 2007). After epidermal lineage commitment, loss of Mi-2 $\beta$  interferes with follicular differentiation but not with differentiation of inter-follicular epidermis (Kashiwagi et al., 2007). In the adult skin, Mi-2 $\beta$  represses genes supporting basal keratinocyte activation, mobilization, and immune cell function (Kashiwagi et al., 2017). Many of the same genes are also induced by physiological challenge to the skin, such as wounding or barrier disruption (Keyes et al., 2016; Lander et al., 2017; Sextius et al., 2010), suggesting that suppression of Mi-2 $\beta$  activity may be a mechanism by which environmental challenges mobilize the skin's stress responses.

Activator protein 1 (AP1) is a family of early response transcriptional complexes comprised of homo- and hetero-dimers between c-JUN and c-FOS family members. AP1 complexes bind to a palindromic 12-O-tetradecanoylphorbol-13-acetate response element and regulate gene expression in response to mitogenic, stress, differentiation, and apoptotic signals (Guinea-Viniegra et al., 2009; Mehic et al., 2005; Risse et al., 1989; Shaulian and Karin, 2002; Wurm et al., 2015). In the basal layer of the skin, the polycomb repressor group complex prevents AP1 from binding and activating terminal differentiation genes expressed in the suprabasal layers. Both the differential expression of AP1 constituents and the suppression of polycomb repressor group complex expression allow for activation of AP1-dependent differentiation and acquisition of epidermal barrier function (Ezhkova et al., 2009).

Here, we show that either barrier disruption or genetic ablation of Mi-2 $\beta$  in the mouse epidermis elicits a transcriptional response that involves similar genes and functional pathways. We show that these distinct physiological and genetic challenges cause a similar increase in chromatin accessibility at enhancers associated with stress response genes that frequently encompass binding sites for AP1. We demonstrate that Mi-2 $\beta$  repressed transcription and activation of AP1 complex components, such as c-JUN, and restricted chromatin access at AP1 binding sites. Increasing activation and occupancy of c-JUN with concomitant loss of Mi-2 $\beta$  at these enhancer sites, which were occupied by JUNB at steady state, correlated with induction of gene expression. A moderate reduction in Mi-2 $\beta$  expression was induced by physiological signals such as barrier disruption that was accompanied by a further albeit selective abrogation of Mi-2 $\beta$  at stress response genes. Permanent loss of Mi-2 $\beta$  caused aberrant induction of AP1, interfered with return to skin homeostasis, and caused severe pathologies. Taken together, our studies support a model by which functional interactions between the chromatin remodeler Mi-2 $\beta$  and the early response complex AP1 account for rapid response and recovery from mechanical injury.

## Results

### Rapid but transient transcriptional responses induced by stress signaling in the epidermis

To examine the molecular mechanisms that control the skin's response to physical insult, we evaluated the effects of acute

stress signaling using a skin barrier disruption assay. Trans-epidermal water loss (TEWL) was measured before and at different time points after removal of the stratum corneum by repetitive tape stripping (TS; Fig. 1, A and B). Immediately after TS, TEWL was significantly increased, but starting at 1 h after treatment, it began to progressively decrease to reach preinjury levels by 48 h (Fig. 1 B). To evaluate gene expression changes during this acute response, basal keratinocytes (ITGA6<sup>+</sup>, CD45<sup>-</sup>, CD34<sup>-</sup>) were sorted before and at different time points after TS and processed for RNA sequencing (RNA-seq; Fig. 1 A and Fig. S1 A; before and at 6, 24, and 96 h after TS). A rapid induction of mRNA changes and subsequent recovery was seen within 96 h after treatment, consistent with the phenotypic changes in TEWL (Fig. 1, C and B; and Fig. S1 B). Notably, most of the transcriptional changes were observed by 6 h after TS, with 1,444 up-regulated and 1,415 down-regulated genes detected (Fig. 1 C and Fig. S1 B). Of the genes induced at 6 h, 70% were no longer elevated at 24 h, and 99% were expressed at preinjury levels by 96 h (Fig. 1 C and Fig. S1 B). A similar rapid response and recovery was seen with down-regulated genes (Fig. 1 C and Fig. S1 B). Gene set enrichment analysis (GSEA) showed induction of different functional pathways early versus later in the response (Fig. 1 D). Genes activated by Myc, the unfolded protein response, and TNF signaling peaked at 6 h, whereas genes involved in MTORC1 signaling, oxidative phosphorylation, and the regulation of the G2M checkpoint peaked at 24 h of the response (Fig. 1 D). Further gene ontology (GO) analysis of all deregulated genes at 6 and 24 h after barrier disruption confirmed participation in cell proliferation, keratinocyte differentiation, and immune cell activation (Fig. S1 C).

Further analysis of differentially expressed genes by K-means clustering revealed induction and suppression of distinct genes and pathways at different time points after barrier disruption (Fig. 1 E and Fig. S1 D). Of the four groups of temporally dysregulated genes identified, genes whose induction peaked as early as 6 h fell within the first two clusters (C1 and C2) and encoded factors required for lipid biosynthesis and keratinocyte terminal differentiation, such as *Abca12*, *Alox12b*, *Aqp3*, *Cldn4*, and *Tgml*; inflammatory mediators, such as *Cxcl1*, *Il24*, *S100a8*, and *S100a9*; and cell proliferation-promoting signals, such as members of the EGF family, *Ereg*, *Areg*, *Tgfa*, *Hbegf*, and *Vegfa* (Fig. 1, E and F, 6 h C1 and C2; Fig. S1 D; and Table S1). Genes induced at a later time point fell into the third cluster (C3) and contained many cell cycle genes, such as *Mki67*, *Ccna2*, *Ccnb1*, *Cdk1*, and *Cdkn3* (Fig. 1 E, 6 h; Fig. S1 D; and Table S1). Notably, genes in this cluster (C3) showed an initial decrease in expression at 6 h, but by 24 h were increased to a higher level relative to steady state, which declined by 96 h. Finally, genes down-regulated early in the response were contained within the fourth cluster (C4) and were associated with circadian rhythm regulation, such as *Per3* and *Cry2*, and lipid metabolism, such as *Acaa2*, *Echs1*, and *Acsc2* (Fig. 1, E and F; Fig. S1 D; and Table S1). These genes were rapidly down-regulated early in the repair process but became reexpressed during the recovery phase. The decrease in the circadian transcriptional regulators *Per3* and *Cry2* may reflect the physiological response to barrier disruption. Whereas reduction of these genes, seen early in the response,

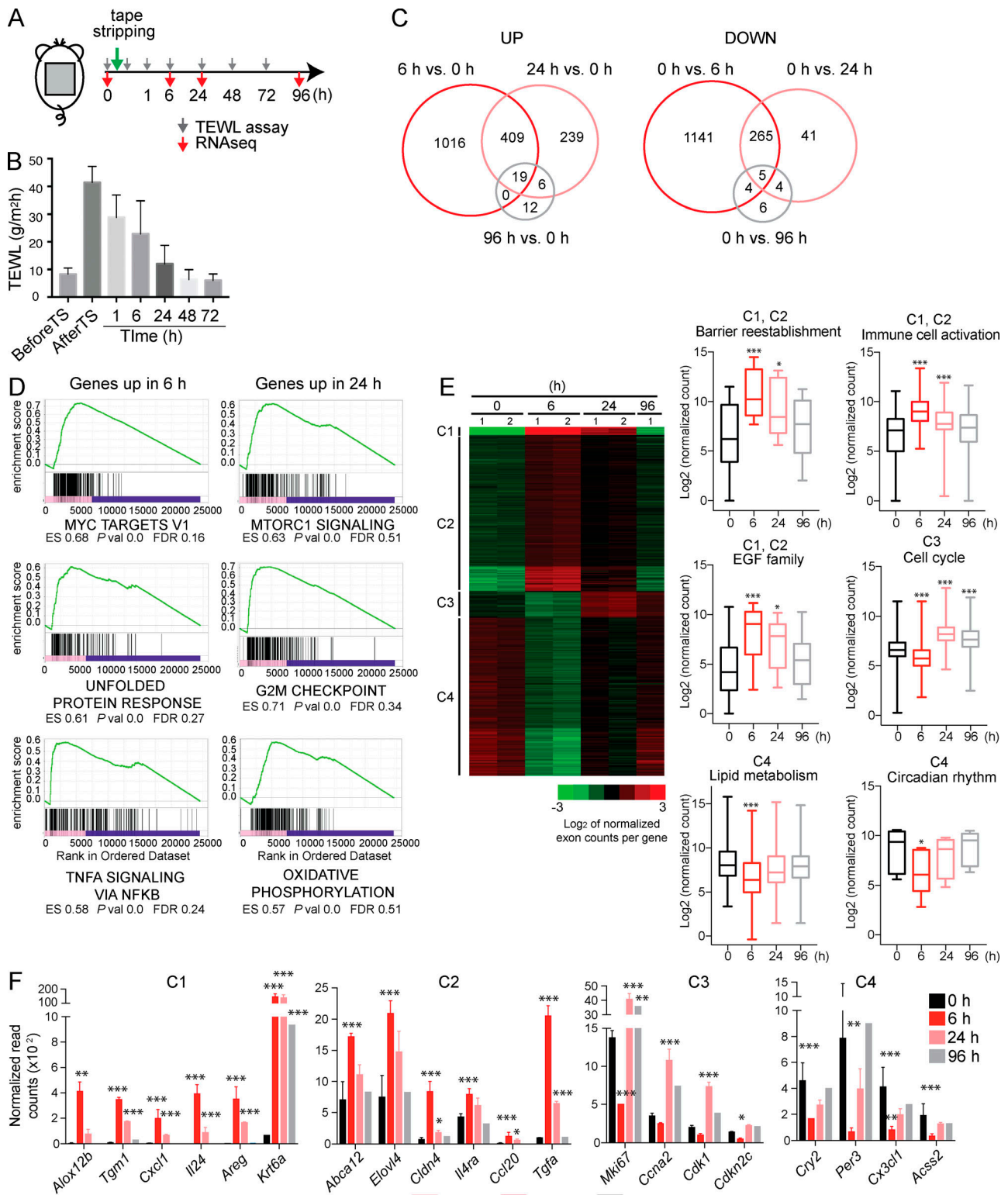


**Figure 1. Rapid induction and repression of genes mediated by barrier disruption. (A)** Experimental approach for barrier disruption studies. Mice with shaved back skin were tape-stripped until TEWL measurements reached 40 g/m<sup>2</sup> · h. Skin was harvested before and at the indicated time points after TS. **(B)** Time course of TEWL before and up to 72 h after TS. TEWL in each group is shown as a bar graph with mean and SEM. **(C)** Overlap of differentially expressed genes at three time points after TS (6, 24, and 96 h) is shown by Venn diagrams ( $|\log_2$  fold change|  $\geq 1$ , FDR < 0.05). Up-regulated genes (UP) are shown on the left and down-regulated genes (DOWN) on the right. **(D)** GSEA comparing up-regulated genes at 6 or 24 h after TS with hallmark gene sets (H) in molecular signature database. Genes induced by Myc, or in response to unfolded proteins or TNF $\alpha$  signaling, were significantly enriched by the 6-h up-regulated subset, whereas genes that support mTORC1 signaling, G2M transition, and oxidative phosphorylation were enriched by the 24-h up-regulated subset. Enrichment profiles are plotted and calculated ES, P values (P val), and FDR are shown. **(E)** Heatmap representation of K-means clustering of differentially expressed genes before and after TS ( $|\log_2$  fold change|  $\geq 1$ , FDR < 0.05). Expression of genes associated with functional categories in each cluster is

shown in box-whisker plots of  $\log_2$  normalized read counts from RNA-seq data. Whiskers extend from the smallest to the largest expression value within each cluster. Expression at 6, 24, and 96 h was compared with 0 h, and P values for expression difference were determined by one-way ANOVA analysis followed by Dunnett's test. \*,  $P < 0.05$ ; \*\*\*,  $P < 0.005$ . **(F)** Expression of representative stress-responding genes as determined by RNA-seq at different time points after TS is shown for each cluster as bar graphs for normalized read counts with mean and SEM. P values for expression differences compared with 0 h were determined by DEseq2 analysis. \*,  $P < 0.01$ ; \*\*,  $P < 0.001$ ; \*\*\*,  $P < 0.0001$ . For TEWL studies (B), four independent experiments were performed with four to six mice per group. Two areas of back skin per mouse were processed for analysis ( $n = 8$ –12 per group). For transcriptional studies (C–F), RNA-seq datasets were generated from two independent experiments with pooled samples from 0 h ( $n = 4$ ), 6 h ( $n = 4$ ), and 24 h ( $n = 4$ ) and from one experiment with pooled samples for 96 h ( $n = 2$ ).

correlates with an increase in keratinocyte proliferation, the increase toward normality, seen later in the response, correlates with epidermal stem cell differentiation. This is in line with previous studies that have shown that changes in core clock genes, such as *Per3* and *Cry2*, predispose epidermal stem cells to environmental cues that regulate proliferation or differentiation (Janich et al., 2013). The down-regulation of lipid metabolism/catabolism genes follows a requirement of keratinocytes to synthesize and secrete lipids into the intercellular space of the cornified layer for reestablishment of the barrier. These genes are also rhythmically regulated, and their expression may reflect changes in *Per3* and *Cry2* expression (Gnocchi et al., 2015).

Thus, barrier disruption triggers the rapid induction of genes involved in barrier reestablishment, cell proliferation, immune cell activation, and repression of genes involved in lipid metabolism and circadian rhythm regulation. Such rapid transcriptional responses appear to be critical for repairing the compromised structural barrier and fortifying the local immune cell defenses. The observed prompt recovery from these transcriptional changes is likely critical for preventing excessive barrier formation and inflammation that can lead to skin pathologies.

### Similar transcriptional response elicited by stress signaling or Mi-2 $\beta$ depletion

Aberrant keratinocyte activation and cell proliferation demarcated by expression of keratin 6 (K6) and Ki67, respectively, were evident shortly after conditional inactivation of the chromatin remodeler Mi-2 $\beta$  in the epidermis (Fig. S2 A; Kashiwagi et al., 2017). Moreover, a highly significant overlap and similar trend in gene expression changes were seen either by barrier disruption or by acute loss of Mi-2 $\beta$  in the epidermis (Fig. 2, A–C;  $P < 0.0001$  by Fisher's exact test; and Table S2). Among the significantly up-regulated genes at 6 h after barrier disruption, 36% were also significantly up-regulated by loss of Mi-2 $\beta$  (Fig. 2, A and B; 524/1,444). By 24 h the number of up-regulated genes declined; however, the relative number shared by Mi-2 $\beta$  loss was further increased (Fig. 2, A and B; i.e., 65%: 439/673). Further examination of the shared significantly up-regulated genes at 6 h and in Mi2 $\Delta$  keratinocytes showed that the majority was still significantly induced at 24 h compared with nonshared genes that were not (Fig. S2 B). These shared genes enriched functional categories such as keratinocyte activation, barrier reestablishment, immune cell activation, and cell growth (Fig. S2 C and Fig. S1 C). Similarly, among the significantly down-regulated genes after 6 h of barrier disruption, 38% (532/1,415) were also significantly down-regulated by loss of Mi-2 $\beta$ , and by 24 h their relative number was further increased (i.e., 54%: 170/315; Fig. 2, A–C).

GSEA comparing significantly up- and down-regulated genes in TS keratinocytes with the transcriptome of Mi-2 $\beta$ -depleted keratinocytes confirmed a similar trend in regulation (Fig. 2 D, false discovery rate [FDR] = 0). Genes up- and down-regulated at both 6 and 24 h strongly correlated with genes up- and down-regulated in Mi-2 $\beta$ -depleted keratinocytes (Fig. 2 D, enrichment score [ES]: 0.752–0.810). The reverse comparison of significantly induced genes upon loss of Mi-2 $\beta$  with the transcriptome of TS keratinocytes showed a weaker correlation (Fig. S2 D, ES: 0.605–0.710), which is consistent with participation of Mi-2 $\beta$  in the repression of genes that are involved in other biological processes in keratinocytes.

### Barrier disruption induces rapid changes in chromatin accessibility

We next examined whether the response to stress signaling was associated with changes in chromatin accessibility. Chromatin accessibility was evaluated genome-wide in sorted keratinocytes before and after barrier disruption or after Mi-2 $\beta$  depletion using the Tn5 transposase assay (assay for transposase-accessible chromatin [ATAC] sequencing [ATAC-seq]; Fig. 3 A). ATAC peaks in TS or Mi-2 $\beta$ -depleted keratinocytes were compared with WT steady-state keratinocytes; if induced, they were classified as differentially induced ATAC (dATACi), and if lost as differentially lost ATAC (dATACl). Similar to the gene expression changes, a rapid gain in dATACi peaks was observed at 6 h after TS that declined by 24 h (Fig. 1 and Fig. 3 B; dATACi peaks: 9,178 at 6 h and 6,262 at 24 h). In sharp contrast to the dATACi peaks, an insignificant number of dATACl peaks was seen at 6–24 h (Fig. 3 B; dATACl peaks: 61 at 6 h and 32 at 24 h; and Tables S3 and S4). The gain in dATACi and loss in dATACl peaks in Mi-2 $\beta$ -depleted keratinocytes by far exceeded what was seen by barrier disruption (Fig. 3 B; dATACi peaks [27,068] and dATACl peaks [1,943]; and Table S5). Nonetheless, a larger number of dATACi compared with dATACl peaks was also seen in Mi-2 $\beta$ -depleted keratinocytes (i.e., >10 fold) as in keratinocytes after barrier disruption.

The majority (~80%) of dATACi peaks observed after Mi-2 $\beta$  depletion or barrier disruption were distributed over intergenic and intronic regions, with only ~10–15% associated with promoters (Fig. 3 C). Moreover, the magnitude of increase in dATACi enrichment was greater at intergenic and intronic regions compared to promoters or exonic regions (Fig. 3 D). These data indicate that barrier disruption or Mi-2 $\beta$  depletion causes a significant reprogramming of regulatory elements that are distal to promoters and may include transcriptional enhancers. It also shows that the detected increase in chromatin accessibility is not just a consequence of a transcriptional increase that should affect promoters as well. Nonetheless, the number and magnitude

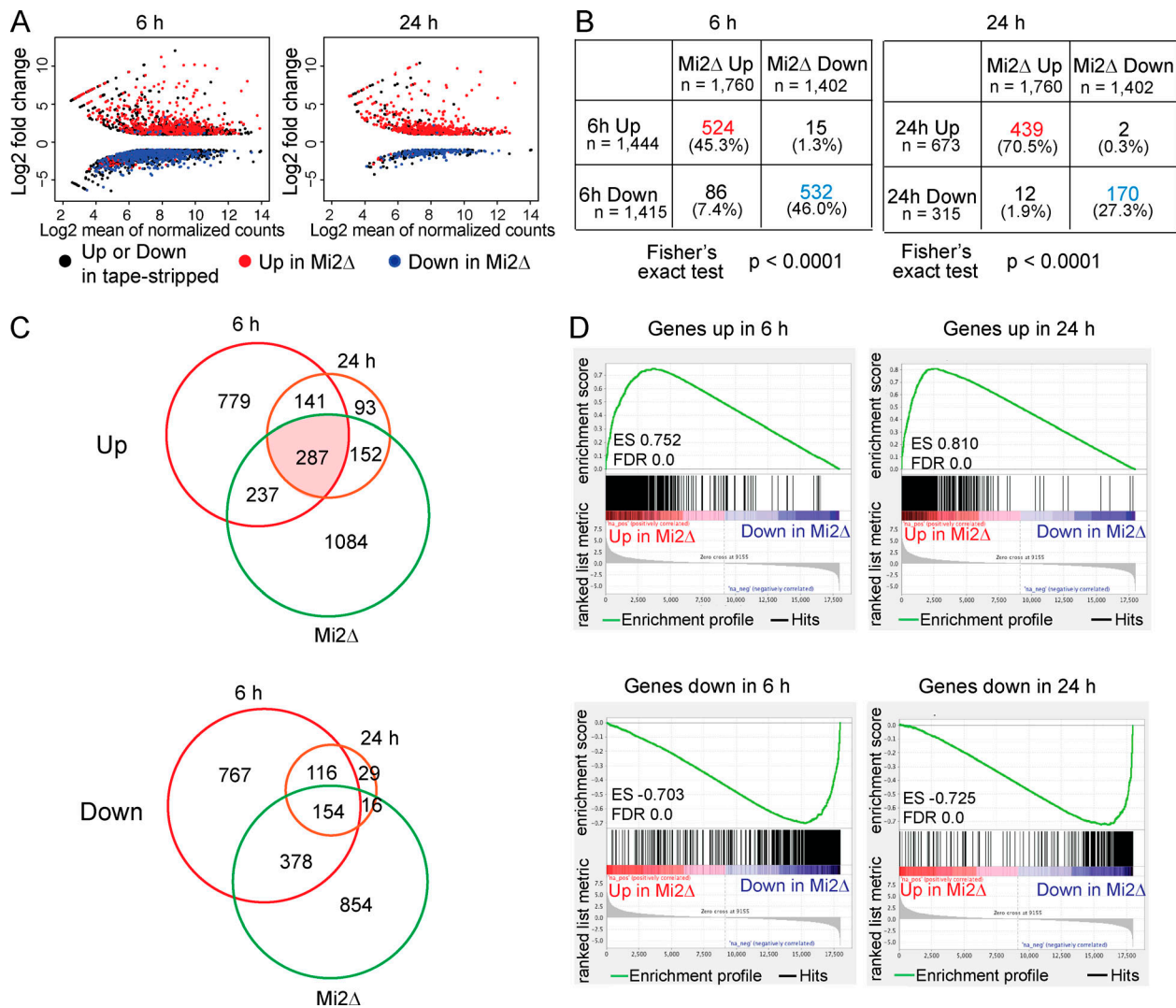


**Figure 2. Common transcription changes induced by stress signaling and Mi-2 $\beta$  depletion.** (A) MA ( $\log_2$  ratio of expression change versus mean average expression) plot of differentially expressed genes ( $|\log_2$  fold change  $\geq 1$ , FDR  $< 0.05$ ) at 6 or 24 h after TS. Mean normalized read counts ( $\log_2$  transformed) are plotted against  $\log_2$  fold change. Shared up- or down-regulated genes with Mi2 $\Delta$  keratinocytes are highlighted in red and blue, respectively. (B) The number of commonly up- (red) or down-regulated (blue) genes after TS (6 or 24 h) and in Mi2 $\Delta$  keratinocytes is shown. A highly significant concordance of differentially expressed genes under the two conditions was calculated by Fisher's exact test ( $P < 0.0001$ ). The percentage of grand total is shown in parentheses. (C) The overlap in differentially expressed genes after TS ( $|\log_2$  fold change  $\geq 1$ , FDR  $< 0.05$ ) or in Mi2 $\Delta$  keratinocytes is shown by Venn diagrams. Up-regulated genes (UP) are shown at the top and down-regulated genes (DOWN) at the bottom. (D) GSEA comparing significantly up- or down-regulated genes at 6 h (top) or 24 h (bottom) after TS with the transcriptional profile of Mi2 $\Delta$  keratinocytes. Enrichment profile is plotted, and calculated ES and FDR are shown. Analysis was performed with RNA-seq datasets generated from the biological replicates described in Fig. 1 and in Kashiwagi et al. (2017).

of change at dATACi peaks was greater in Mi-2 $\beta$ -depleted keratinocytes compared with keratinocytes after barrier disruption (Fig. 3, B and D).

The potential contribution of TFs to the barrier disruption response was tested by de novo motif analysis of all dATACi peaks obtained at 6 or 24 h after TS (Fig. 3 E). AP1 complex motifs were most significantly associated with induced regulatory sites (Fig. 3, E and F). Other factors associated with dATACi at 6 or 24 h were CEBP and KLF5, albeit at a lower frequency and P value compared with AP1 (Fig. 3 E). Enrichment of dATACi peaks with STAT3, a key regulator of keratinocyte proliferation and migration, was seen at 24 h, consistent with the later increase in epidermal proliferation (Fig. S2 A and Fig. 1 D; Sano

et al., 2005). The dATACi peaks in Mi-2 $\beta$ -depleted keratinocytes were also significantly enriched for AP1 motifs (Fig. 3, E and F). In addition to AP1, a highly significant enrichment of NFY, OCT, and KLF5 motifs was seen at dATACi peaks from Mi-2 $\beta$ -depleted keratinocytes (Fig. 3 E). The association of OCT and KLF5, TFs essential for maintaining keratinocyte cell identity (Ge et al., 2017; Racila et al., 2011), with Mi-2 $\beta$ -regulated chromatin sites suggest that Mi-2 $\beta$  participates in a wider transcriptional network involved in both stress responses and keratinocyte differentiation.

Taken together, our studies show that barrier disruption causes a rapid and highly significant gain in chromatin accessibility that correlates with the rapid induction of stress

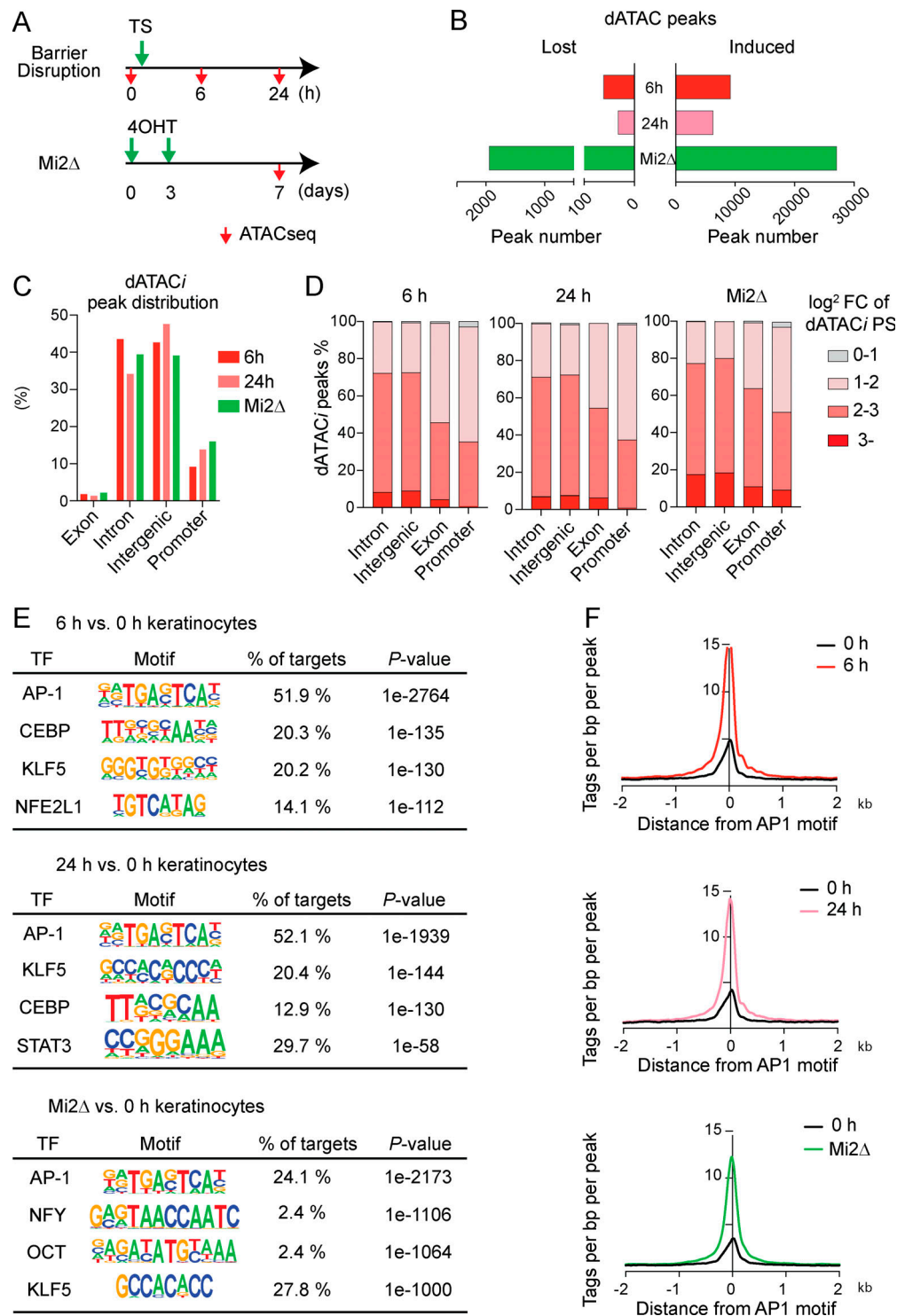


**Figure 3. Barrier disruption-induced chromatin changes and associated TFs.** (A) Experimental approach for ATAC studies after barrier disruption or Mi-2 $\beta$  depletion in keratinocytes. Back skin was harvested before and at the indicated time points after TS or Mi-2 $\beta$  depletion, and sorted keratinocytes were processed for ATAC-seq. (B) dATACi or dATACi peaks in TS or Mi2 $\Delta$  keratinocytes compared with WT keratinocytes are shown by histograms (6 h: red; 24 h: pink; and Mi2 $\Delta$ : green). (C) Genomic annotation of dATACi peaks at 6 or 24 h after TS or in Mi2 $\Delta$  keratinocytes revealed a similar genome-wide distribution. (D) Distribution of dATACi changes ( $\log_2$  of dATACi peak score [PS]) at annotated genomic locations in TS (6 or 24 h) or Mi2 $\Delta$  keratinocytes. dATACi peaks were subdivided into four subsets with low to high peak scores (0–1, 1–2, 2–3, 3+), represented by color shading within the respective histograms. FC, fold change. (E) De novo motif (Homer) discovery reveals potential TF association with dATACi peaks in TS (6 or 24 h) or Mi2 $\Delta$  keratinocytes. P value for motif discovery and % of peaks (targets) with motif are shown. (F) Read density (reads per bp per peak) at dATACi peaks with AP1 motif detected in TS (6 or 24 h) or Mi2 $\Delta$  keratinocytes relative to WT. ATAC-seq datasets were generated from two independent experiments with pooled samples at 0 h ( $n = 4$ ), 6 h ( $n = 4$ ), and 24 h ( $n = 4$ ) and from Mi2 $\Delta$  mice ( $n = 4$ ) in A–F.

response genes. The very small number of sites with reduced chromatin accessibility detected does not correlate with the large number of down-regulated genes, indicating that the loss in expression was not due to a change in chromatin structure. Finally, the similar genome-wide distribution of sites with gained chromatin accessibility and AP1 enrichment detected by either Mi-2 $\beta$  loss or barrier disruption strongly supports a role for this chromatin remodeler in the skin's response to damage.

### Stress signaling-induced chromatin changes are regulated by Mi-2 $\beta$

We further evaluated the mechanism that controls induction of chromatin accessibility after barrier disruption or Mi-2 $\beta$  loss. We examined the temporal nature of chromatin changes induced at 6 or 24 h after TS and after Mi-2 $\beta$  loss. K-means clustering was performed with ATAC-seq datasets centered on dATACi peaks obtained at 6 or 24 h after TS (Fig. 4, A–D). In all five clusters, the increase in chromatin accessibility seen at 6 h after TS was reduced by 24 h (Fig. 4, A and B). These chromatin changes strongly correlated with the rapid induction of gene expression observed in response to barrier disruption (Fig. 1). On the other hand, three of the dATACi peak clusters (Fig. 4 C; C1, C2, and C4) seen at 24 h displayed a similar increase in chromatin accessibility at 6 h, indicating rapid induction but also maintenance of accessibility. This is consistent with the maintenance of induced expression for a subset of stress response genes (Fig. 2 C). Two of the dATACi clusters that were specifically induced at 24 h (Fig. 4, C and D; C3 and C5), were associated with cell cycle genes such as *Ccnh*, *Ccnli*, and *Cdk14* expressed later in the response, as shown in Fig. 1, E and F.

Notably, in four of the dATACi clusters detected at 6 h after barrier disruption (C1, C3, C4, and C5) that displayed little chromatin accessibility at steady state,  $\geq 50\%$  of the peaks were associated with AP1 motifs (Fig. 4 E). In contrast, peaks of the C2 cluster that were already accessible at steady state showed a much lower association with AP1. Furthermore, whereas  $\sim 1/3$  of the C2 peaks were associated with promoters, very little promoter association (on average  $< 5\%$ ) was observed for the other four clusters that were strongly associated with AP1 motifs (Fig. 4 E). Three of the five dATACi clusters detected at 6 or 24 h showed overlap with dATACi peaks in Mi-2 $\beta$ -depleted keratinocytes (Fig. 4, A–D). Moreover,  $\sim 65\text{--}80\%$  of the genes associated with dATACi peaks upon barrier disruption also displayed either overlapping or associated dATACi peaks upon Mi-2 $\beta$  loss (Fig. 4 F and Fig. S3 A). Thus barrier disruption or Mi-2 $\beta$  loss caused similar changes in chromatin accessibility at regulatory sites located in the vicinity of stress response genes.

Genes associated with an increase in chromatin accessibility displayed a significant and progressive increase in expression from 6 to 24 h (Fig. 4 G). Genes that were up-regulated at 6 h after barrier disruption were also tested for their association with dATACi peaks (Fig. 4 H and Table S4). 33% of the induced genes at 6 h after TS were associated with dATACi peaks at this time point. An additional 28% of these genes were also associated with dATACi peaks induced by genetic ablation of Mi-2 $\beta$  (Fig. 4 H). A majority (84%) of the genes induced at 6 h that were associated with dATACi peaks after TS were also

associated with dATACi peaks after Mi-2 $\beta$  deletion. Furthermore, genes that were commonly induced by barrier disruption or Mi-2 $\beta$  depletion showed an even greater association (i.e., 89%) with dATACi peaks caused by Mi-2 $\beta$  deletion (Fig. 4 H). A very strong enrichment with dATACi peaks caused by Mi-2 $\beta$  loss or TS (i.e., 91–95%) was also observed for up-regulated genes at 24 h after barrier disruption (Fig. S3 B, 24 h).

*Il24*, an activator of MAPK and STAT3 signaling in keratinocytes, *Cldn4*, *Krt17*, and *Ngf*, are examples of stress response genes whose expression is normally repressed by Mi-2 $\beta$  in the steady state (Fig. 4 I and Fig. S3 C). In these cases, a rapid increase in chromatin accessibility at upstream or intragenic sites was detected upon barrier disruption or Mi-2 $\beta$  loss that correlated with rapid induction in gene expression. In some cases, the promoters were already in an accessible state that was not greatly increased by either barrier disruption or Mi-2 $\beta$  loss.

Thus, changes in chromatin accessibility occur rapidly after stress response signaling is induced in keratinocytes. Some of these chromatin changes are dissipated rapidly while others are maintained. A highly significant number of these stress response-induced regulatory sites also respond to Mi-2 $\beta$  depletion in keratinocytes and are associated with genes induced during both processes, implicating this chromatin remodeler as a negative effector in their regulation.

### Mi-2 $\beta$ -dependent mechanism of regulation is conserved between mouse and human

Mi-2 $\beta$ , an ATP-dependent chromatin remodeler, represses expression of genes normally induced by stress response signaling in keratinocytes, in part by restricting access at promoter-distal regulatory sites associated with putative AP1 binding sites. A potential direct role for Mi-2 $\beta$  in this molecular process was tested by establishing its chromatin distribution in both mouse and human cultured primary keratinocytes and in an immortalized human keratinocyte cell line (HaCaT) by chromatin immunoprecipitation (ChIP) sequencing (ChIP-seq).

A highly significant overlap was seen for genes associated with Mi-2 $\beta$  chromatin enrichment sites ( $P < 2.77 \times 10^{-68}$ ) in mouse and human keratinocytes (Fig. 5 A and Tables S6 and S7). Shared genes contributed to biological pathways involved in immune cell activation, epithelial cell proliferation and differentiation, cell adhesion, and EGFR and MAPK signaling (Fig. 5 B). Genomic annotation of Mi-2 $\beta$  chromatin enrichment sites revealed that  $> 70\%$  were distributed at non-promoter sites in both mouse and human keratinocytes (Fig. 5 C). De novo motif analysis of Mi-2 $\beta$  enrichment sites in chromatin from mouse or human keratinocytes again implicated AP1 as a major Mi-2 $\beta$  functional partner (Fig. S4 A). Furthermore, a majority of genes induced at 6–24 h (i.e., 64–65%) after barrier disruption in the mouse epidermis were directly bound by Mi-2 $\beta$  (Fig. 5 D). An even greater association with Mi-2 $\beta$  (82%) was seen for genes commonly induced by barrier disruption (6–24 h) and Mi-2 $\beta$  loss in mouse epidermis (Fig. 5 D). Additionally, 73% of these commonly repressed genes in mouse keratinocytes were also bound by Mi-2 $\beta$  in human keratinocytes (Fig. 5 D).

To further evaluate the Mi-2 $\beta$ -based mechanisms, we knocked-down Mi-2 $\beta$  mRNA with shRNA lentiviral vectors in

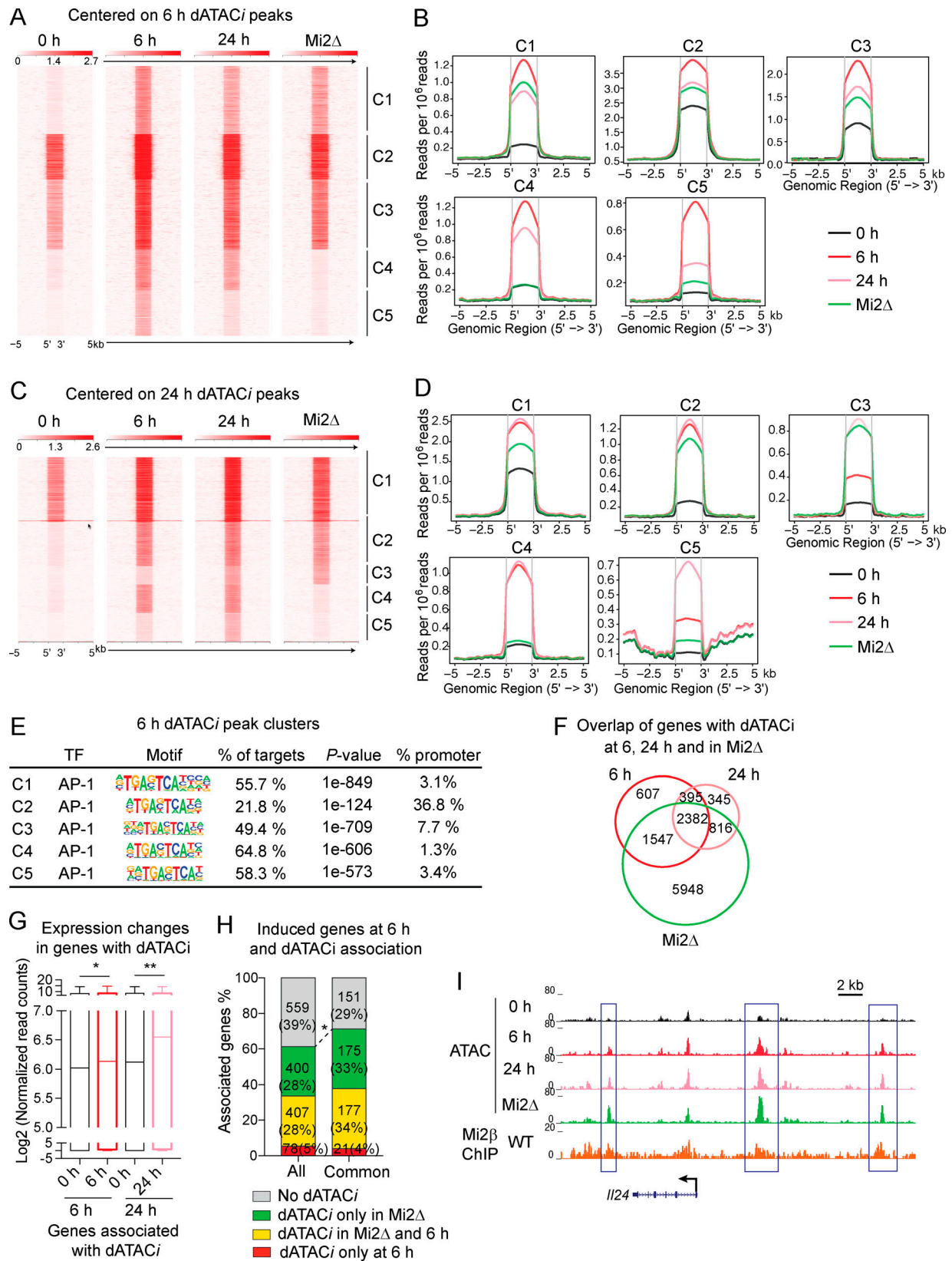


Figure 4. **Common changes in chromatin induced by stress signaling and Mi-2β depletion.** (A) Heatmap of K-means clustering of ATAC-seq datasets from 0 h (before TS), 6 h, or 24 h after TS and from Mi2Δ keratinocytes centered on dATACi peaks identified after 6 h of TS. C1, 2,311 peaks; C2, 1,545 peaks; C3, 2,365 peaks; C4, 1,389 peaks; C5, 1,568 peaks. (B) Histograms of read densities (read count per million mapped reads) plotted at ±5 kb from the dATACi peaks identified at 6 h after TS for the five clusters (C1–C5) shown in the heatmap in A and color-coded for the four ATAC-seq datasets (0 h, 6 h, 24 h, and Mi2Δ keratinocytes). (C) Heatmap of K-means clustering of ATAC-seq datasets from 0, 6, or 24 h after TS and Mi2Δ keratinocytes centered on dATACi peaks



identified at 24 h in TS keratinocytes. C1, 2,190 peaks; C2, 1,490 peaks; C3, 639 peaks; C4, 974 peaks; C5, 974 peaks. **(D)** Histograms of read densities (read count per million mapped reads) plotted at  $\pm 5$  kb from the dATACi peaks identified at 24 h after TS for the five clusters (C1–C5) shown in the heatmap in C and color-coded for four ATAC-seq datasets (0 h, 6 h, 24 h, and Mi2 $\Delta$  keratinocytes). **(E)** Percentage of dATACi peaks with AP1 motifs and promoter association is shown for each of the five clusters (C1–C5) identified at 6 h after TS together with P values for motif discovery. **(F)** Venn diagram depicting the overlap of genes associated with dATACi peaks identified after TS (6 or 24 h) or after Mi2 $\Delta$  depletion in keratinocytes. **(G)** Expression of genes associated with dATACi peaks is shown as a box-whisker plot of log<sub>2</sub> normalized read counts from RNA-seq data from 6 or 24 h after TS. The whiskers extend from the smallest to the largest expression value within each group. Significance in difference in expression was obtained by a two-tailed unpaired t test; \*, P < 0.005; \*\*, P < 0.0005. **(H)** Bar graph depicting the frequency and number of all significantly up-regulated genes ( $|\log_2$  fold change|  $\geq 1$ , FDR < 0.05) after 6 h of TS that were also associated with dATACi peaks at the same time point and/or with dATACi peaks in Mi2 $\Delta$  keratinocytes. Genes with dATACi peak association under one (Mi2 $\Delta$ : green; 6 h: red), both (yellow), or neither (gray) condition are color coded. A similar presentation is provided for genes that were commonly up-regulated at 6 h after TS and in Mi2 $\Delta$  keratinocytes. Commonly up-regulated genes had a higher significant association with dATACi peaks compared with all up-regulated genes (\*, P < 0.0001 determined by Fisher's exact test). **(I)** Genome browser tracks on *IL24*, showing increased chromatin accessibility (ATAC-seq) after TS (6 or 24 h) or in Mi2 $\Delta$  keratinocytes. Mi-2 $\beta$  ChIP-seq in mouse primary cultured keratinocytes is also shown. Mi-2 $\beta$  peaks associated with dATACi peaks are depicted as blue rectangles. Analysis was performed with ATAC-seq and RNA-seq datasets described in Figs. 3 and 1. ChIP-seq for Mi-2 $\beta$  was performed from primary mouse keratinocytes generated from newborn mice after brief expansion in culture.

cultured normal human keratinocytes (NHKs; Fig. 5 E and Fig. S4 B). Cultured keratinocytes replicate aspects of in vivo basal keratinocytes and are amenable to mechanistic studies. ChIP-seq studies for histone modifications and TFs were performed with both control (CTR) and Mi-2 $\beta$ -depleted (Mi2KD) primary human keratinocytes (Fig. 5 E and Fig. S4 C). Regulatory elements associated with Mi-2 $\beta$  were established by K-means clustering of histone modifications at Mi-2 $\beta$  binding sites in NHK chromatin (Fig. 5 F). Mi-2 $\beta$  distribution was detected at promoters (C2: marked by both H3K27Ac and H3K4me3), in the vicinity of promoters (C1 and C5: H3K27Ac and H3K4me3), and at promoter-distal enhancers (C3: marked only by H3K27Ac; Fig. 5 F). Upon Mi-2 $\beta$  depletion, enhancers (C3) associated with Mi-2 $\beta$  exhibited an increase in enrichment for H3K27Ac and RNA polymerase II (RNAPII), indicating a potential increase in activity (Fig. 5, F and G). The preferential increase in transcriptionally permissive histone modifications at Mi-2 $\beta$ -associated enhancers compared with promoters in NHKs is reminiscent of the significant increase in Mi-2 $\beta$ -associated dATACi peaks at promoter-distal sites in mouse keratinocytes, indicating a conserved mechanism of regulation (Fig. 3 C). No change in the already strong H3K4me3 enrichment was seen at the Mi-2 $\beta$ -associated promoters (Fig. 5, F and G, C2: promoter). The Mi-2 $\beta$ -associated C3 enhancers were significantly enriched for AP1 motifs, although enrichment for p63, TEAD, and CEBP binding was also observed at lower frequency (Fig. 5 H). Genes associated with the Mi-2 $\beta$  C3 enhancers were involved in leukocyte activation, establishment of endothelial barrier, epidermal differentiation, and MAPK signaling and were up-regulated upon Mi-2 $\beta$  loss (Fig. 5 I). About 1/3 of the genes associated with Mi-2 $\beta$ -bound enhancers displayed binding of Mi-2 $\beta$  at their promoter regions (Fig. S4 D).

Thus, Mi-2 $\beta$  serves as the central node of a conserved epigenetic mechanism that directly controls expression of gene networks that are involved in both the response to stress signaling and keratinocyte differentiation.

#### Antagonism between Mi-2 $\beta$ and stress response signaling in the regulation of AP1

Normally repressed enhancers associated with Mi-2 $\beta$  in NHKs were enriched for AP1 motifs, suggesting a potential antagonism between Mi-2 $\beta$  and an activated AP1 complex (Fig. 5 H). AP1

motifs were also highly enriched at enhancers induced by barrier disruption in mouse keratinocytes and upon Mi-2 $\beta$  depletion (Figs. 3 and 4). In addition, among the genes directly bound by Mi-2 $\beta$  in NHKs was c-JUN and in mouse keratinocytes Jun and JunB (Fig. 6, A and B).

Upon Mi-2 $\beta$  knockdown (Mi2KD) in NHKs, a rapid increase of c-JUN mRNA, protein, and protein phosphorylation were seen from early to later time points after Mi-2 $\beta$  depletion (Fig. 6, C and D; c-JUN and phosphorylated-c-JUN [p-c-JUN] at days 3 and 5 in Mi-2 $\beta$ KD). In contrast to c-JUN, JUNB was expressed in NHKs and displayed a small increase at the protein level at 3 d after Mi-2 $\beta$  depletion and a small reduction at 5 d (Fig. 6 D; JUNB day 3 versus day 5). However, in mouse ex vivo keratinocytes, induction of JunB mRNA and protein were reproducibly seen both after Mi-2 $\beta$  depletion and TS (Fig. 6, E and F). Although an increase in c-Jun mRNA was not reproducibly seen after Mi-2 $\beta$  depletion or TS in mouse keratinocytes, a strong increase at the protein and phosphorylation level were detected (Fig. 6 F). Mi2 $\Delta$  mouse epidermis was also tested for c-Jun protein expression by immunostaining. c-Jun expression was augmented at the basal and suprabasal layer of the epidermis as well as at the granular layer, where AP1 is normally involved in terminal differentiation (Fig. 6 G). Thus, loss of Mi-2 $\beta$  or mechanical stress causes rapid induction of AP1 factors in basal keratinocytes in support of stress signaling.

#### Functional interactions between Mi-2 $\beta$ and AP1 in human keratinocytes

We next tested the chromatin distribution of JUNB and c-JUN before and after Mi-2 $\beta$  depletion in NHKs (Fig. 7, A–C). Whereas JUNB enrichment peaks were readily detected in NHKs, a very small number of c-JUN peaks were present, consistent with the very low level of c-JUN expression in these cells (Fig. 7 A, Fig. 6, C and D; and Table S8). De novo c-JUN peaks dramatically increased upon Mi2KD in NHKs and overlapped with the majority of JUNB peaks observed in CTR NHKs (Fig. 7, B and C). Motif analysis of JUNB and c-JUN peaks in NHKs before and after Mi2KD confirmed binding through AP1 motifs that were distributed predominantly at promoter distal sites (Fig. S5, A and B). Co-clustering of JUNB (NHK/CTR), c-JUN (NHK Mi2KD), and Mi-2 $\beta$  (NHK and HaCaT) ChIP-seq datasets at de novo c-JUN peaks detected after Mi2KD revealed co-occupancy of JUNB

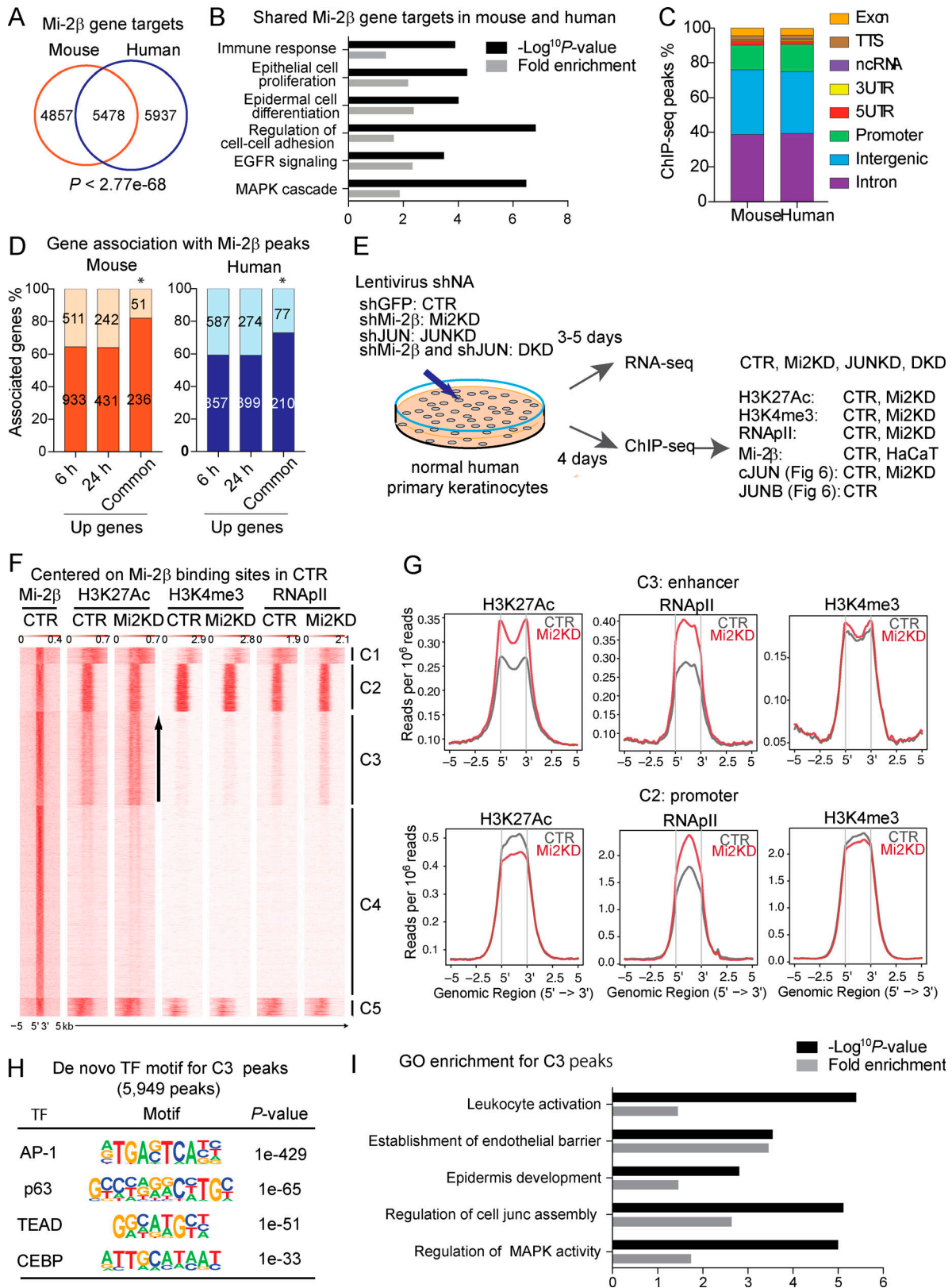


Figure 5. **Conserved mechanism of Mi-2 $\beta$  regulation in keratinocytes.** (A) Overlap of genes associated with Mi-2 $\beta$  enrichment peaks in mouse and human keratinocytes is shown. A highly significant P value  $< 2.77 \times 10^{-68}$  for the overlap between the two gene sets was calculated by Fisher's exact test. (B) Pathway analyses of genes associated with Mi-2 $\beta$  enrichment peaks in both mouse and human keratinocytes. Select GO pathways and associated P values ( $-\log_{10}$ ) with fold enrichment are shown. (C) Genome distribution of Mi-2 $\beta$  peaks in mouse and human keratinocytes reveals a similar association with annotated genomic elements. (D) Bar graph depicting the frequency and number of significantly ( $|\log_2$  fold change  $\geq 1$ , FDR  $< 0.05$ ) up-regulated genes after TS (6 or 24 h) that are

also associated with Mi-2 $\beta$  enrichment peaks in mouse (left) and human (right) keratinocytes. The frequency of association with Mi-2 $\beta$  peaks was significantly higher for the subset of genes commonly up-regulated at both 6 and 24 h after TS and in Mi2 $\Delta$  keratinocytes (shared) as determined by Fisher's exact test (\*,  $P < 0.0001$ ). **(E)** Experimental design for knockdown of Mi-2 $\beta$  in primary NHKs by lentiviral shRNA transduction and further studies on transcriptome (RNA-seq), chromatin, and TF landscapes (ChIP-seq). **(F)** Heatmap of K-means clustering analysis of ChIP-seq data for Mi-2 $\beta$ , histone modifications (H3K27Ac and H3K4me3), and RNAPII from CTR and Mi2KD human primary keratinocytes, centered on Mi-2 $\beta$  enrichment peaks from the same cells. C1, C2, and C5 were marked by H3K4me3, H3K27Ac, and RNAPII and identified as promoters or promoter-proximal regions. C3 associated with weak H3K27Ac and RNAPII signal but not with H3K4me3 and was identified as a cluster of poised enhancers. The upward arrow indicates an increase in H3K27Ac upon Mi2KD. **(G)** An increase in enrichment for H3K27Ac and RNAPII, detected upon Mi2KD in C2 and C3, is shown as histograms of read densities (read count per million mapped reads) plotted over the C2 promoter and C3 enhancer clusters. No change in the high level of H3K4me3 detected at the C2 promoters was seen upon Mi2KD. **(H)** De novo motif discovery for potential TFs associated with Mi-2 $\beta$  peaks in C3 and P values for discovery are shown. **(I)** Pathway analyses of up-regulated genes after Mi2KD in NHKs that are associated with C3 enhancers. Select GO pathways and associated P values ( $-\log_{10}$ ) with fold enrichment are shown. ChIP-seq datasets were generated from primary NHKs expanded in culture and infected with shRNA CTR or shRNA for CHD4 (Mi-2 $\beta$ ). One of two representative ChIP-seq experiments is shown.

and Mi-2 $\beta$  at these sites in NHKs (Fig. 7, B and C). Although co-occupancy by JUNB and Mi-2 $\beta$  was detected at the chromatin level in NHKs, stable interaction between these factors was not readily seen off chromatin (Fig. S5 C). Upon Mi2KD, an overall increase in H3K27ac was detected in the vicinity of JUNB and c-JUN enrichment peaks, a majority of which were bound by Mi-2 $\beta$  in NHKs and HaCaTs (Fig. 7, B and C; and Fig. S5 D). Up-regulated genes associated with de novo c-JUN peaks in Mi2KD NHKs supported pathways of cell adhesion, migration, signaling, and proliferation that are also induced by stress responses (Fig. 7 D).

The functional contribution of c-JUN to genes induced by loss of Mi-2 $\beta$  in NHKs was tested. Gene expression changes between NHKs transfected with a CTR shRNA vector and NHKs transfected with shRNAs for CHD4 (Mi-2 $\beta$ ), c-JUN, or CHD4 and c-JUN were compared (Fig. S5 E, Fig. 7 E, and Table S9). About 1/4 (419/1,611) of the genes up-regulated upon Mi2KD showed a significant reduction in expression by concomitant knockdown of c-JUN (Fig. S5 E and Fig. 7 E). These reverted genes showed a highly significant association with c-JUN peaks compared with non reverted genes as calculated by a  $\chi^2$  test (Fig. 7, F and G;  $P = 0.001$ ). Furthermore, Mi-2 $\beta$  was more significantly enriched in the proximity of genes that were induced by its loss and bound by c-JUN compared with genes that were induced but not bound by c-JUN (Fig. 7 H;  $P = 0.0001$ ). *COL7A1*, *RARA*, and *PLB1* are examples of direct targets of Mi-2 $\beta$  and c-JUN that are regulated by the two factors in a reciprocal fashion (Fig. 7 I and Fig. S5, F and G).

In conclusion, these studies reveal a dynamic interaction between Mi-2 $\beta$  and the heterogeneous collection of protein heterodimers collectively referred to as the AP1 complex. Under homeostatic conditions in human keratinocytes, an AP1 complex containing JUNB co-localizes with Mi-2 $\beta$  on repressed genes that include those encoding alternative AP1 complex components. Stress signaling or Mi-2 $\beta$  depletion relieve the repression and allow an activating AP1 complex to promote gene expression. The antagonism between Mi-2 $\beta$  and this activating AP1 complex contributes to timely abatement of stress responses.

### Mi-2 $\beta$ response to and recovery from barrier disruption

Our studies indicate that Mi-2 $\beta$  holds the genes of the stress response in a repressed state and that abrogation of Mi-2 $\beta$  activity induces their expression by activating AP1.

However, stress response genes are only a subset of the genes held repressed by Mi-2 $\beta$  in the epidermis. Thus, if interference with Mi-2 $\beta$  is the mechanism by which stress response genes are activated, there must be a selective reduction of Mi-2 $\beta$  activity at these loci.

To test this hypothesis, we first examined Mi-2 $\beta$  expression during the stress response. A consistent, albeit, small reduction in Mi-2 $\beta$  mRNA was detected at 6 h after TS (Fig. 8 A). Immunostaining for Mi-2 $\beta$  protein in the skin also showed a decrease in the nuclei of the basal epidermis (Fig. 8 B). A small reduction in Mi-2 $\beta$  activity can sensitize its direct gene targets to additional mechanisms that antagonize its activity. Indeed, when we tested whether Mi-2 $\beta$  chromatin occupancy was altered during the stress response by ChIP-quantitative PCR (qPCR) at candidate Mi-2 $\beta$  gene targets that are induced during the response, a significant reduction in Mi-2 $\beta$  occupancy at 6 h after barrier disruption was seen that correlated with an increase in expression (Fig. 8 C). *JunB*, *Alox3*, *Mapk6*, and *Ppid* were genes induced by barrier disruption in vivo that showed Mi-2 $\beta$  occupancy in cultured and ex vivo mouse keratinocytes. All exhibited a significant reduction in Mi-2 $\beta$  chromatin occupancy at 6 h after TS (Fig. 8 C). In contrast, Mi-2 $\beta$  occupancy at candidate loci whose expression was not affected by TS (e.g., *Krt14* and *Myod1*) remained unaltered (Fig. 8 C).

Thus, induction of the response to barrier disruption may involve selective abrogation of Mi-2 $\beta$  activity at a subset of responder genes. Consistent with this model, Mi-2 $\beta$  activity was not required for an initial recovery of barrier function after TS (Fig. 8 D; mice treated 2 $\times$  with 4-OHT before TS). Prior to barrier disruption, TEWL was at a similar low level in both WT and Mi-2 $\beta$  mutant skin (Fig. 8 E). After barrier disruption, a similar rapid recovery from TEWL was observed under both conditions (Fig. 8 E; 1–6 h). However, if Mi-2 $\beta$  is a critical repressor of these genes, then the resolution of the response should depend on Mi-2 $\beta$  activity. Since mice with efficient deletion of Mi-2 $\beta$  in the epidermis did not survive the additional stress of the TS procedure, mice with mosaic deletion of Mi-2 $\beta$  in the epidermis that tolerate the stress response were used for evaluation of the resolution phase (Fig. 8 D; mice treated once with 4-OHT before TS). A clear difference in skin phenotype was observed at 4–5 d after TS, with severe desquamation observed in the tape-stripped compared with noninjured areas in Mi-2 $\beta$  mutant skin (Fig. 8 G). Histological analysis showed mild thickening of WT epidermis at 24 h that returned to normal thickness by 5 d

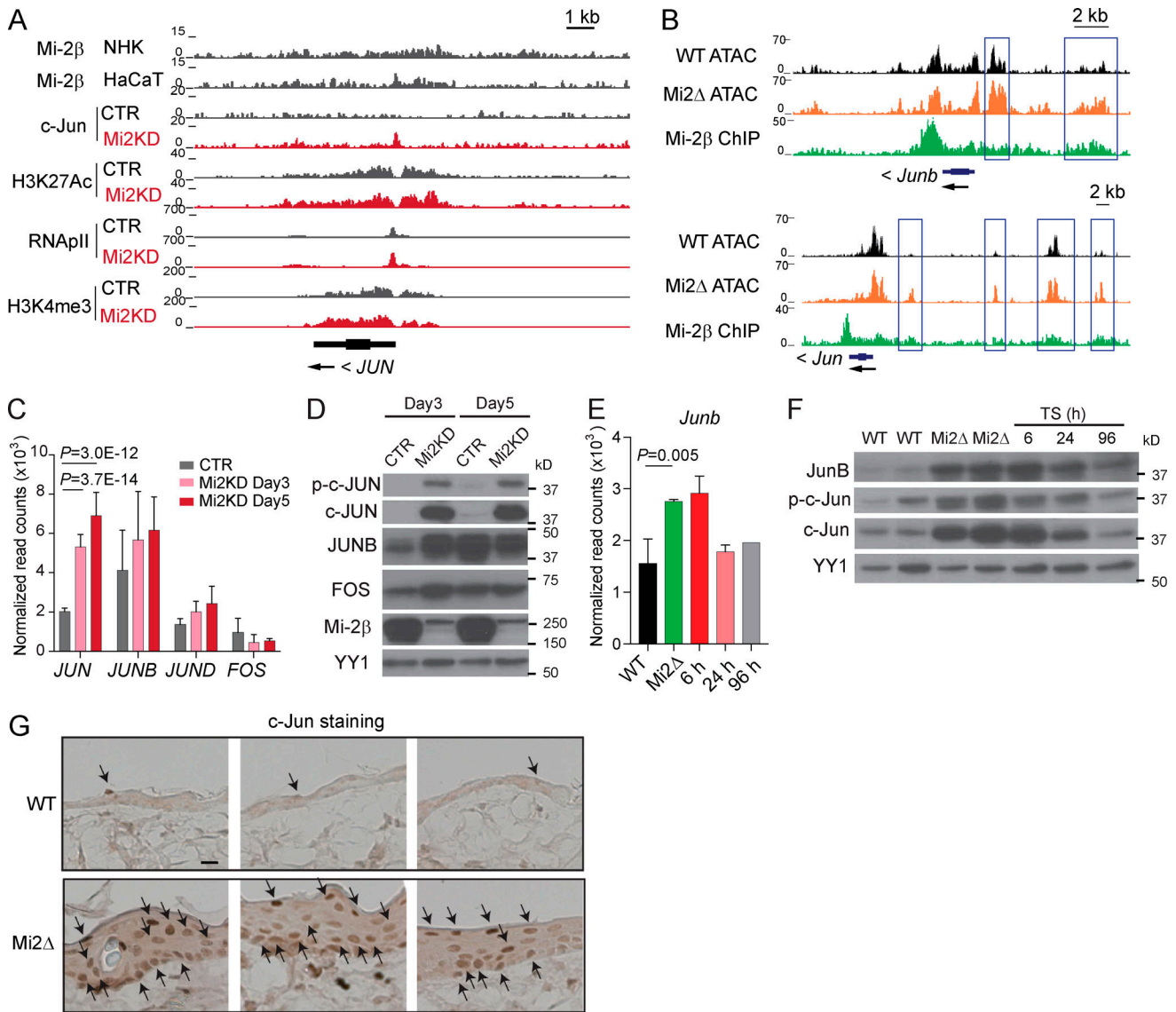


**Figure 6. Transcriptional and post-transcriptional regulation of AP1 factors in keratinocytes.** (A) Genome browser tracks at the *JUN* locus showing normalized ChIP-seq reads for Mi-2β in NHKs and in the HaCaT cells, and for JUN, H3K27Ac, RNAPII, and H3K4me3 in CTR (black histogram) and Mi2KD (red histogram) NHKs. (B) Genome browser tracks at the *Junb* locus showing normalized ATAC-seq reads from ex vivo WT and Mi2Δ keratinocytes, and ChIP-seq for Mi-2β in primary mouse keratinocytes. (C and D) Expression of *JUN*, *JUNB*, *JUND*, and *FOS* mRNAs (P values as determined by DESeq2; C) and immunoblotting for p-c-JUN, c-JUN, JUNB, FOS, Mi-2β, and YY1 (loading control; D) in CTR and Mi2KD primary NHKs at days 3 and 5 after shRNA lentiviral transduction. The experimental procedure is described in Fig. 5 E. (E and F) Expression of *JunB* mRNA (P value as determined by DESeq2; E) and immunoblotting of JunB, p-c-Jun, c-Jun, and YY1 (loading control; F) in WT, Mi2Δ, and TS (6, 24, and 96 h) ex vivo mouse keratinocytes. (G) Immunohistochemistry for c-Jun in WT and Mi2Δ epidermis. Scale bar = 10 μm. Arrows point to nuclei with c-Jun expression. ChIP-seq, ATAC-seq, and RNA-seq were performed as described in Figs. 1, 3, 4, and 5. Immunoblot data shown in D and F are representative of three independent experiments. Immunostaining of c-Jun shown in G is representative of three independent experiments with three WT and three Mi2Δ mice.

(Fig. S2 A and Fig. 8 F). In agreement with histology, expression of K6 and Ki67 in WT epidermis was induced at 6–24 h after TS but returned to a preinjury level by 5 d after treatment (Fig. S2 A and Fig. 8 G; WT tape-stripped day 5). In sharp contrast, Mi-2β mutant epidermis showed a severe and persistent increase in thickness and keratinization after TS compared with noninjured areas (Fig. 8 F). Further increase in Ki67-positive cells and strong K6 expression was seen in Mi2β mutant epidermis at 5 d after TS (Fig. 8 G; Mi2Δ mosaic tape-stripped day 5).

In summary, a selective reduction of Mi-2β activity at rapidly responding genes appears to be a key early event in stress signaling. Nonetheless, reduction in Mi-2β activity is short-lived, and Mi-2β repression is rapidly reinstated for skin to return to homeostasis and normal differentiation. Upon constitutive, instead of a normally transient, loss of Mi-2β, epidermis appears to be over-repairing the disrupted barrier by hyperproliferation and hyperkeratinization, manifestations of aberrant skin differentiation.

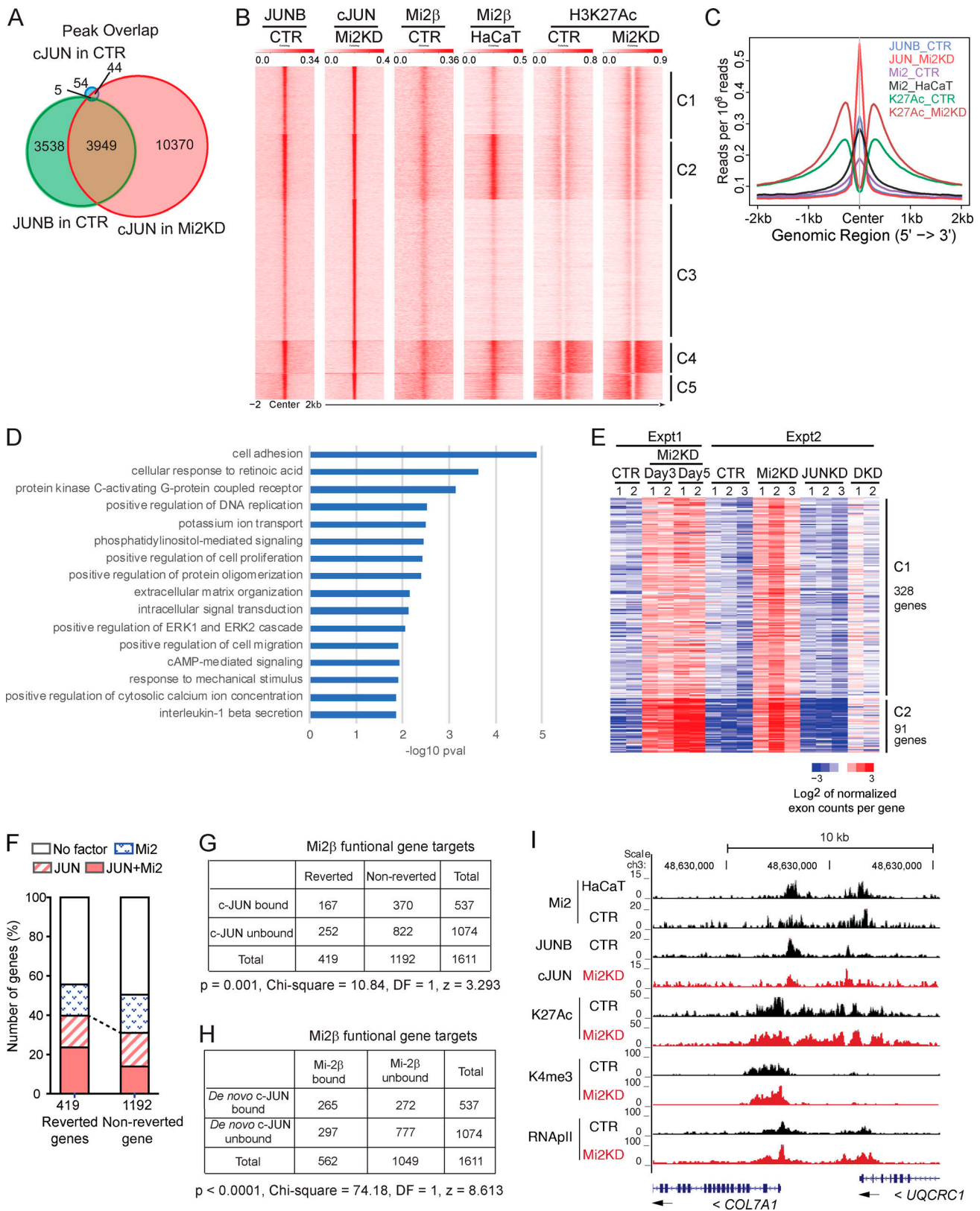


Figure 7. **Functional antagonism between AP1, an early response complex, and Mi-2β in keratinocytes.** (A) Venn diagram depicting the overlap of c-JUN peaks identified in CTR NHKs (blue) or Mi2KD NHKs (red) and JUNB peaks identified in CTR NHKs (green). (B) Heatmap of K-means clustering analysis of ChIP-seq data for JUNB in CTR, c-JUN in Mi2KD, Mi-2β in CTR and HaCaT, and H3K27Ac from CTR NHKs and Mi2KD NHKs, centered on de novo c-JUN peaks detected after Mi2KD. (C) Occupancy (read count per million mapped reads) of TFs (JUNB, JUN, and Mi-2β) and H3K27Ac at de novo c-JUN peaks ( $\pm 2$  kb) as described in B is shown by histogram format. (D) Pathway analyses of up-regulated genes associated with cJUN enrichment peaks in Mi2KD NHKs. Select GO pathways and

associated P values ( $-\log_{10}$ ) are shown. **(E)** Heatmap of K-means clustering analysis for a subset of significantly induced genes after Mi2KD ( $|\log_2$  fold change  $\geq 1$ , FDR  $< 0.05$ ), which revert to normal levels after concomitant knockdown of c-JUN ( $|\log_2$  fold change  $< 0$ ,  $P < 0.05$ ). See also Fig. S5 D for all significantly induced genes in Mi2KD. Normalized expression is shown in CTR, Mi2KD, c-JUN knockdown (c-JUNKD), and Mi2KD and c-JUNKD (DKD) NHKs. Data from two experiments each with two or three replicates in each are shown. Expt, experiment. **(F)** Among the genes de-repressed in Mi2KD NHKs (days 3–5), the frequency of genes bound by Mi-2 $\beta$  in CTR NHKs (blue) and bound by de novo c-JUN peaks in Mi2KD NHKs (pink stripes) and genes bound by both Mi-2 $\beta$  in CTR NHKs and c-JUN in Mi2KD NHKs (pink) are depicted as bar graphs. **(G)** Statistical evaluation of genes induced by loss of Mi-2 $\beta$ , positively regulated by c-JUN and bound by c-JUN. Induced genes that were reverted by concomitant knockdown of c-JUN were significantly associated ( $P = 0.001$ ) with c-JUN peaks compared with induced genes that were not reverted. Data from  $\chi^2$  analysis (two-sided) are shown. DF, degrees of freedom. **(H)** Statistical evaluation of association of genes induced by loss of Mi-2 $\beta$  with c-JUN and Mi-2 $\beta$  binding. Induced genes that were bound by c-JUN were also significantly enriched for Mi-2 $\beta$  binding ( $P$  value 0.0001) compared with induced genes targets that were not bound by c-JUN. Data from  $\chi^2$  analysis (two-sided) are shown. **(I)** Genome browser tracks of normalized ChIP-seq reads for TFs (JUNB, JUN, Mi-2 $\beta$ , and RNAPII) and histone modifications (H3K27Ac and H3K4me3) generated from NHKs (CTR, black histogram), Mi2KD NHKs (red histogram) and HaCaT cells (black histogram) are shown at the *COL7A1* locus. ChIP-seq for JUNB and JUN was performed on one set of CTR and Mi2KD primary NHKs. RNA-seq for CTR, Mi2KD, JUNKD, and DKD was performed twice with duplicates or triplicate samples in each experiment.

## Discussion

Skin, as our interface to the outside world, is constantly exposed to environmental challenges to which it responds by inducing signaling and transcriptional programs that mend the structural barrier while placing the immune system on high alert. Both rapid induction and subsequent repression of stress responses are critical for preserving normal skin function by engaging signaling and TFs as well as chromatin regulators to work in concert toward this goal. Here, we show that Mi-2 $\beta$ , the nucleosome remodeler of the NuRD complex, is a key regulator of this process that functions by restricting chromatin access at enhancers associated with stress response genes, many of which contain AP1 binding sites. Our data support a model by which a transcriptionally repressive AP1 complex based on JUNB acts with Mi-2 $\beta$  to locally repress at these enhancer sites. Stress signaling displaces Mi-2 $\beta$  from these loci and may be sufficient to initiate stress response gene expression, de-repression and activation of c-JUN, and replacement of a repressive by an activating AP1 complex that may amplify the response (Fig. 9).

Previous studies have shown that loss of Mi-2 $\beta$  in the epidermis causes keratinocyte activation and skin inflammation in the absence of an overt differentiation defect, suggesting that Mi-2 $\beta$  and the NuRD complex play a critical role in regulating the skin's stress responses (Kashiwagi et al., 2017). To test this hypothesis, we characterized both the transcriptional and chromatin response to skin barrier disruption induced by TS and compared it with that of Mi-2 $\beta$  loss in keratinocytes in vivo. A highly significant overlap in the induction of genes involved in epidermal barrier reestablishment, EGFR signaling, keratinocyte proliferation, and immune cell activation was seen under both conditions in mouse keratinocytes. A rapid induction of chromatin accessibility sites and gene expression changes observed upon barrier disruption indicated a mechanism of transcription regulation that incorporates active chromatin remodeling. The majority of newly accessible regulatory sites were located at promoter-distal areas and were also induced by loss of Mi-2 $\beta$  in the epidermis, thereby supporting a role of this chromatin remodeler in their regulation. These putative stress response enhancers were significantly enriched for AP1 binding sites, suggesting that Mi-2 $\beta$  holds the stress response genes in a poised state by restricting their access (Fig. 9). This hypothesis was examined in detail using cultured keratinocytes from both human and mouse skin. Mi-2 $\beta$  chromatin enrichment sites were

associated with transcriptional enhancers encountered at both differentiation and stress response genes before their activation.

AP1 is a transcriptional activator that is comprised of dimers formed between members of the JUN and FOS families that are differentially expressed in the basal and suprabasal layers of the skin (Welter and Eckert, 1995). AP1 family members regulate keratinocyte proliferation and differentiation and are also involved in the wound-healing process (Adhikary et al., 2004; Efimova et al., 2004; Takahashi et al., 2002). Aberrant activation of AP1 has been implicated in skin pathological conditions such as carcinogenesis and disease development caused by chronic inflammation (Kolev et al., 2008; Zenz et al., 2005). Mi-2 $\beta$  directly repressed expression of c-JUN and JUNB mRNAs in human and mouse keratinocytes, respectively. In addition, an increase in JunB and Jun protein and phosphorylation were detected in the basal layer of mouse epidermis after Mi-2 $\beta$  depletion or barrier disruption. Nonetheless, in NHKs, JUNB but not c-JUN was expressed and occupied many enhancers that were also enriched for Mi-2 $\beta$ . Upon loss of Mi-2 $\beta$ , these enhancers became occupied by activated c-JUN and displayed an increase in chromatin accessibility and transcription of associated genes. The coexistence of JUNB with Mi-2 $\beta$ -NuRD at AP1 sites suggests the existence of an AP1 transcription-repressive complex that upon stress signaling is replaced by an AP1 transcription-activating complex (Fig. 9). This model is supported by a previous study that demonstrated that repression of gene expression was mediated by c-JUN/NuRD complex interaction in colon cancer epithelial cells, and that this interaction and the gene repression were disrupted by JNK signaling (Aguilera et al., 2011). The transient nature of a transcription-activating AP1 complex may permit rapid reactivation of Mi-2 $\beta$  and rerepression of stress response genes.

The polycomb-PRC2 complex is another epigenetic regulator of keratinocyte differentiation that functions in part by antagonizing AP1 activity (Ezhkova et al., 2009; Wurm et al., 2015). PRC2 is highly active in basal keratinocytes, where it restricts access to AP1 sites required for expression of keratinocyte differentiation genes, such as those of the epidermal differentiation complex (Ezhkova et al., 2009; Wurm et al., 2015). In suprabasal cells, PRC2 expression is diminished, allowing AP1 to access enhancers supporting epidermal differentiation complex expression and stratification. While these chromatin-based mechanisms of restricting AP1 activity are similar, there is a major mechanistic difference. Whereas the loss of PRC2

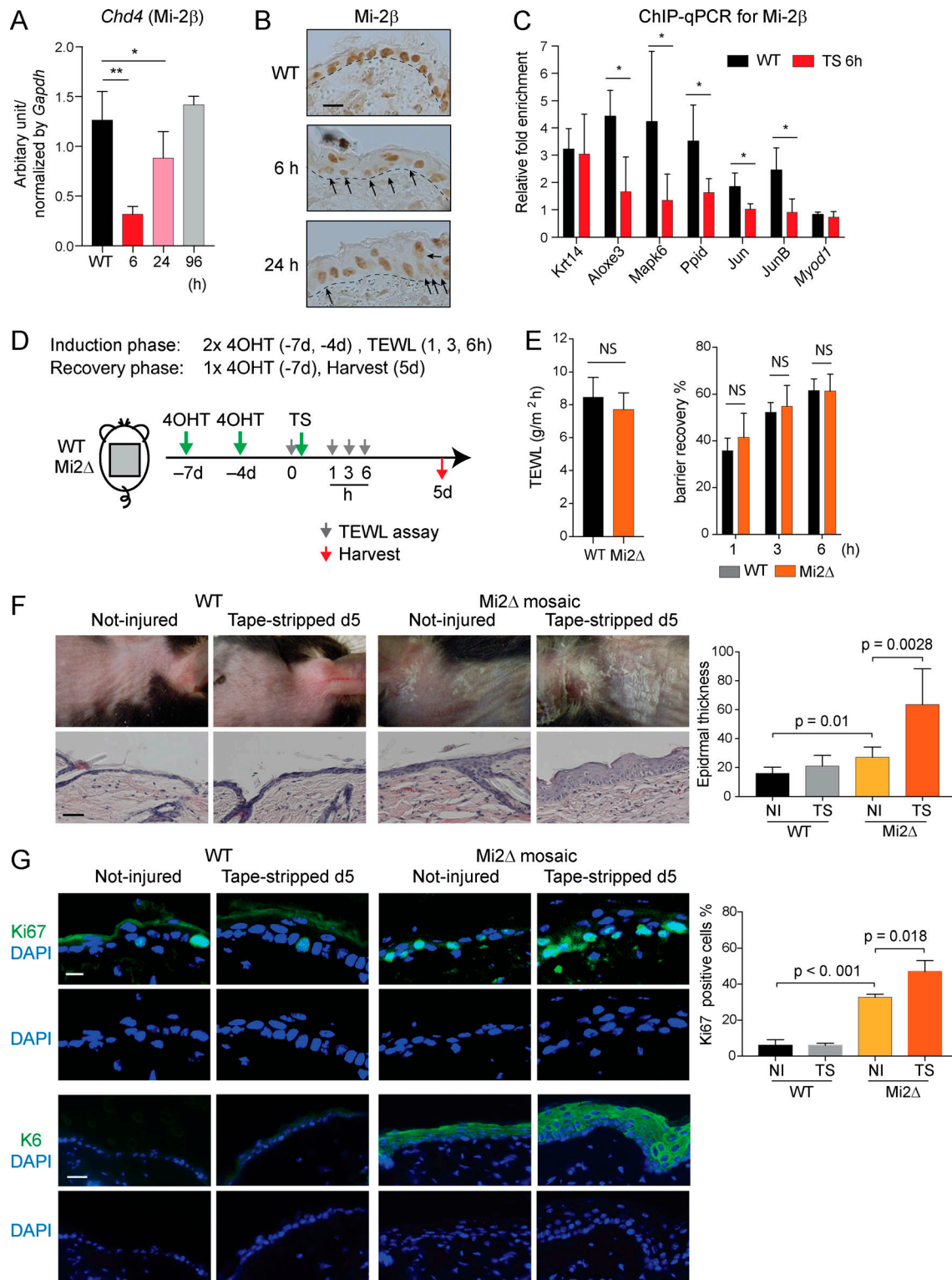


Figure 8. **Dynamic regulation of Mi-2β plays a key role for the induction of stress response and the recovery to homeostasis.** (A) A transient decrease in *Chd4* (Mi-2β) expression was detected by RNA-seq during the time course of TS and was validated by qPCR. The means and SEM of expression data in each group of qPCR samples are shown ( $n = 3$  for each group). \*,  $P < 0.01$ ; \*\*,  $P < 0.005$  (one-way ANOVA followed by Dunnett's test). (B) Immunohistochemistry for Mi-2β protein expression in WT and tape-stripped (6 and 24 h) epidermis. Scale bar = 10 μm. Arrows point to nuclei with reduced Mi-2β expression. (C) ChIP-qPCR for Mi-2β at select target sites associated with stress response genes (e.g., *Aloxes3*, *Mapk6*, *Ppid*, *Jun*, and *JunB*) at 6 h after TS. *Krt14* was used as a positive control bound by Mi-2β but not affected by its deletion, and *Myod1* was used as a negative control not bound by Mi-2β. Relative fold enrichment with mean and SEM is shown ( $n = 5$  for each gene target tested by ChIP-qPCR). Significance in enrichment (\*,  $P < 0.05$ ) was calculated by a two-tailed unpaired t test. (D) Experimental design for testing the induction and recovery phase after TS in WT and *Mi2Δ* mice. For evaluating the induction phase, depletion of *Mi2Δ* in the epidermis was performed by two i.p. injections of 4-OHT (days -7 and -4). For evaluating the recovery phase, mosaic depletion of *Mi-2β* in the epidermis

was achieved by one i.p. injection of 4-OHT (day -7). WT and Mi2Δ mice were then tape-stripped (day 0), and skin was harvested and evaluated by histochemistry and immunofluorescence (day 5). **(E)** TEWL was measured before (day 0; left) and up to 6 h after TS of WT and Mi2Δ mice (right). The change in TEWL at the indicated time point (1, 3, and 6 h) after TS was calculated as a percentage of the change immediately after TS. Means and SEM for data points in each group are shown ( $n = 8$  for each group). **(F)** Representative phenotypes (upper panel) and H&E staining (lower panel) of WT and Mi2Δ mosaic skin at 5 d after barrier disruption are shown (left). Not-injured (NI) areas in WT and Mi2Δ mosaically depleted skin are shown as controls. Epidermal thickness measurements are shown in a bar graph (right) with mean and SEM ( $n = 5$  for each group). P values were calculated by one-way ANOVA followed by Dunnett's test. Scale bar = 25  $\mu\text{m}$ . **(G)** Immunofluorescence detection for Ki67 (top) and K6 (bottom) expression in regions with or without barrier disruption in WT and Mi2Δ mice (left). The percentage of Ki67-positive cells in each group is shown as a bar graph with mean and SEM (right;  $n = 4$  for each group). P values were calculated by one-way ANOVA followed by Dunnett's test. Scale bar = 10  $\mu\text{m}$  (Ki67) and 25  $\mu\text{m}$  (K6). qPCR data of three experiments with a total of three mice per group are shown in A; immunohistochemistry shown in B is from one representative of three independent experiments performed with a total of three mice per group; ChIP-q-PCR shown in C is from two experiments with a total of five WT mice and five mice from 6 h after TS; TEWL data shown in E are from four independent experiments with a total of four to six mice per group. Histological studies shown in F and G are representative of two independent experiments with a total of five mice per group.

associated with terminal keratinocyte differentiation is permanent, Mi-2 $\beta$  activity is transiently overridden in the basal layer to allow a rapid stress response and subsequent recovery.

The strong overlap in gene expression and chromatin changes observed during barrier disruption and Mi-2 $\beta$  depletion establish the importance of this chromatin remodeler in holding genes poised to respond to challenge and suggest that abrogation of Mi-2 $\beta$  may be a mechanism by which these genes are activated. However, not all genes regulated by Mi-2 $\beta$  in the epidermis are activated in response to barrier disruption. In addition to a decrease in Mi-2 $\beta$  transcription and protein after TS, we observed a selective decrease in Mi-2 $\beta$  occupancy at genes induced by stress response *in vivo*. The general reduction in Mi-2 $\beta$  expression may cooperate with enhanced expression or activation of TFs like AP1 to tip the balance of competition between repression and activation selectively at gene loci occupied

by these factors. Other genes dependent on Mi-2 $\beta$  for repression may remain silent if the TFs responsible for their induction are not activated. In that context, it is perhaps noteworthy that the subset of stress response genes that also respond to Mi-2 $\beta$  deletion remain expressed longer than the subset that does not. The incorporation of a positive feedback loop (that attenuates Mi-2 $\beta$  expression) to tip this balance may take longer to reverse than a mechanism supporting induction of stress response genes that are not repressed by Mi-2 $\beta$ . Consistent with a repressive role of Mi-2 $\beta$  in the reestablishment of skin barrier function, its loss did not affect this process upon mechanical injury. However, even mosaic depletion of Mi-2 $\beta$  in the epidermis caused too much repair and regeneration of the disrupted barrier, with excessive proliferation and keratin production that resulted in hyperkeratosis and acanthosis. Thus, rapid restoration of Mi-2 $\beta$  activity is necessary for transient

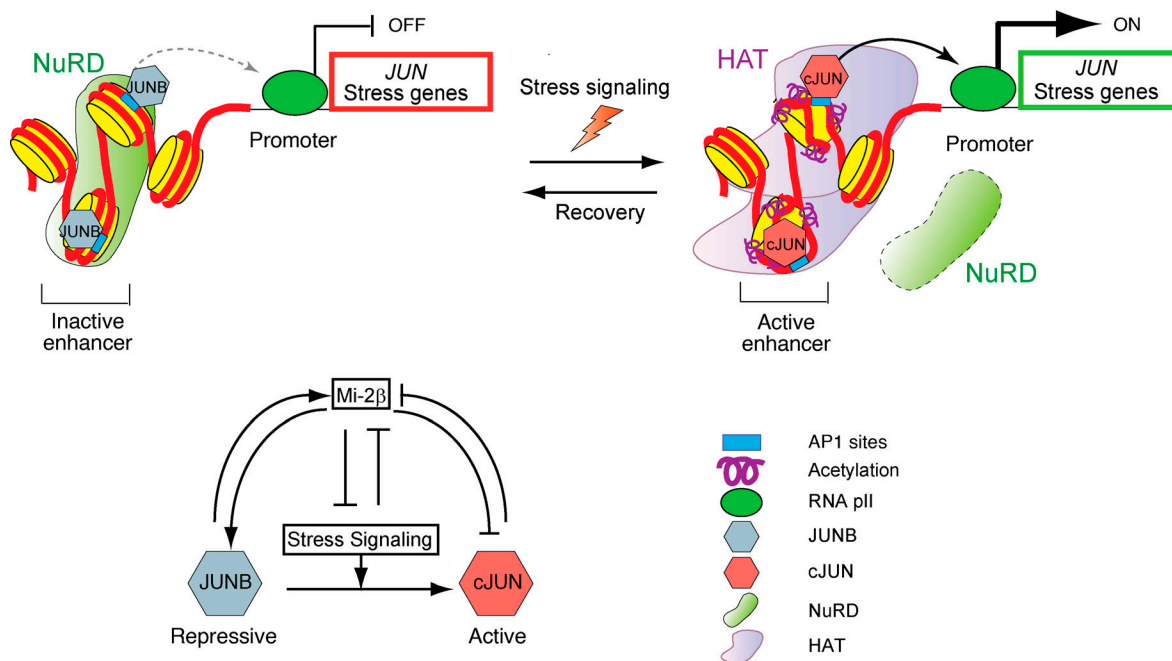


**Figure 9. A model of regulation of stress signaling by Mi-2 $\beta$ .** Mi-2 $\beta$  and JUNB co-occupancy at AP1 sites provide a transcriptionally repressive complex that restricts chromatin and expression of stress response genes including c-JUN. Reduction of Mi-2 $\beta$  by physical or genetic insult causes induction and recruitment of c-JUN at AP1 sites that increase chromatin accessibility and transcription, possibly by displacing Mi-2 $\beta$  and/or by recruiting chromatin modifiers such as histone acetyltransferases (HATs). The transient nature of activation of the c-JUN complex allows for rapid reinstatement of Mi-2 $\beta$ -JUNB repressive activities at AP1 sites and rerepression of stress response genes.



activation of stress response signaling and normal keratinocyte differentiation.

In conclusion, our studies provide a new working model for the mechanisms that permit rapid response to skin challenge and return to epidermal homeostasis (Fig. 9). Of the genes induced by mechanical barrier disruption, roughly half depend on Mi-2 $\beta$  activity to remain repressed in normal epidermis. For this Mi-2 $\beta$ -repressed gene subset, the challenge results in a transient and local reduction in Mi-2 $\beta$  activity, which, in concert with augmented expression of transcription-activating factors such as c-JUN, elicits a rapid response. These chromatin changes and the transcriptional response to stress are short-lived, as is the signaling that supports c-JUN activation; Mi-2 $\beta$  activity is rapidly reinstated, and the balance is shifted back to gene repression. The antagonistic interplay between epigenetic and transcriptional regulators was well established here, but the mechanism by which Mi-2 $\beta$  repressive activity is reinstated in a timely fashion at the end of the stress response remains to be elucidated. While the changes in AP1 phosphorylation and composition summarized in Fig. 9 are formally sufficient, interactions between Mi-2 $\beta$  and other transcriptional regulators bound nearby may also contribute to the reestablishment of repression. The discovery of key nodes in the regulatory network that controls keratinocyte homeostasis presented in these studies provides access to these questions. Our detailed characterization of the genomic response to barrier disruption also identifies genes that may be regulated by distinct mechanisms.

While our effort to confirm the relevance of this work in mice to human skin was confined to studies *in vitro*, it is noteworthy that a study of newly accessible chromatin sites in xenografted human skin equivalents after TS also identified AP1 as a likely regulator of the barrier disruption response (Lander et al., 2017). In addition, microarray analysis of gene expression changes in human skin after barrier disruption is consistent with the results reported here (Sextius et al., 2010). This suggests that our work, which provides a mechanism by which an AP1-regulated response may be mobilized in response to stress, may be translated to new approaches to target chronic skin conditions in which a failure to repress the stress response leads to a range of skin disease and cancer.

## Materials and methods

### Mice

Mi-2 $\beta$ <sup>loxF/loxF</sup> mice were generated in the Georgopoulos laboratory (Williams et al., 2004) and bred to the *Krt14-CreERT2* transgenic mice as previously described (Kashiwagi et al., 2017). Mi-2 $\beta$ <sup>loxF/loxF</sup> *Krt14-CreERT2* transgenic mice used in this study were backcrossed to C57BL/6 mice more than six times. C57BL/6 mice were used for TS. Mice were 8–12 wk old at the time of analyses. Gene inactivation was achieved by two *i.p.* injections of mice with 0.5 mg of 4-OHT (Sigma-Aldrich) with a 3-d interval. This protocol was used to generate keratinocyte samples for RNA-seq and ATAC-seq studies and to study the role of Mi-2 $\beta$  in the initial recovery phase of barrier function after TS. To examine the role of Mi-2 $\beta$  in the return to homeostasis after barrier disruption, mice were delivered a single *i.p.*

injection of 4-OHT to achieve mosaic deletion of Mi-2 $\beta$  before TS. All animal experiments were performed according to protocols approved by the Subcommittee on Research Animal Care at Massachusetts General Hospital (Charlestown, MA) and in accordance with the guidelines set forth by the US National Institutes of Health.

### Mechanical injury by barrier disruption

Barrier disruption by TS was performed with 20–50 strokes of transparent tape on the shaved back skin until TEWL reached 40 grams per square meter per hour (g/m<sup>2</sup> · h). For evaluation of barrier recovery, TEWL was measured before ( $x$ ) and at 0 ( $y$ ), 1 ( $z1$ ), 3 ( $z2$ ), and 6 ( $z3$ ) h after barrier disruption. The recovery rate was calculated by  $y - z$  ( $z1$ ,  $z2$ , or  $z3$ )/ $y - x \times 100$  (%). Skin was harvested for RNA-seq and ATAC-seq at the indicated time points (before and at 6, 24, 96, and 120 h after TS).

### Cell isolation and sorting

Dorsal epidermis was separated from the dermis by digestion with 0.25% trypsin overnight at 4°C to obtain a single-cell suspension. Cells were stained with anti-CD45 (30-F11), anti-CD34 (RAM34), and anti-ITGA6 (eBioGoH3; eBioscience or BD Pharmingen). ITGA6<sup>+</sup>, CD45<sup>-</sup>, and CD34<sup>-</sup> cells were sorted with a FACS Aria (BD Biosciences) and used for further analyses.

### Keratinocyte cell cultures

Primary human epidermal keratinocytes were isolated from three independent de-identified neonatal foreskin samples (a gift from Drs. Rachael A. Clark and Jessica E. Teague, Brigham and Women's Hospital, Boston, MA). Briefly, a single-cell suspension was obtained from foreskin by incubation with 2 U/ml Dispase II (Roche) overnight at 4°C, followed by incubation with 0.25% trypsin (Gibco) for 10 min at 37°C. For primary mouse keratinocytes, cells were prepared from newborn skin by digestion with 0.25% trypsin (Gibco) overnight at 4°C. Primary keratinocytes were cultured under serum-free conditions with keratinocyte growth medium (Gibco). HaCaT cells were cultured in DMEM supplemented with 10% FCS.

### Lentiviral gene transduction

The shRNA lentiviral constructs for Mi-2 $\beta$ , c-JUN, and CTR were obtained from Mission shRNA (Sigma-Aldrich). Transfection into HEK293T cells and lentiviral production were performed as described previously ((Hu et al., 2016). For transduction into primary NHKs, cells were incubated with the infection medium containing lentiviral particles for 6 h and then replaced with fresh medium containing 1  $\mu$ g/ml puromycin (Sigma-Aldrich). Cells were then selected for 3–5 d in puromycin and used for further studies.

### Histology, immunofluorescence, and immunohistochemistry

Samples were fixed in 4% paraformaldehyde overnight at 4°C and then embedded in paraffin. Tissues were sectioned at 5  $\mu$ m and stained with hematoxylin and eosin after de-paraffinization. For immunofluorescence, sections were de-paraffinized and then used for antigen retrieval using a citrate-based buffer (Vector). The primary antibodies used for staining were rabbit

polyclonal Ki67 (Abcam) and rabbit polyclonal K6 (BabCo). Alexa Fluor 488 conjugated anti-rabbit antibodies (Cell Signaling) were used for secondary antibodies, and DAPI (Vector) was used for counterstaining nuclei. For immunohistochemistry, a mouse monoclonal Mi-2 $\beta$  (16G4; Millipore; Kim et al., 1999) was used as a primary antibody. The MOM Fluorescent kit (Vector) was used for staining. Sections were incubated with the avidin-biotin-peroxidase complex and then stained with 3,3'-Diaminobenzidine (Vector). Images were taken with a Nikon A1 confocal microscope or a Zeiss Axio Scan.

### RNA-seq and data analysis

RNA-seq datasets were generated from two independent experiments using  $10^6$  cells for mouse sorting keratinocytes (Figs. 1, 2, and 4) and  $2 \times 10^6$  cells for human primary keratinocytes expanded in culture (Figs. 5 and 7). Total RNA was extracted with a Direct-zol RNA kit (Zymo Research). The Truseq stranded mRNA sample prep kit (Illumina) was used for the construction of cDNA libraries for RNA-seq. The libraries were single-end sequenced using the Illumina HiSeq 2000 platform at the Bauer Center Systems Biology Core at Harvard University or the Illumina NextSeq 550 at the Cutaneous Biology Research Center. Read alignment was performed on the mm10 or hg19 assembly of the mouse or human genome respectively with the STAR genome alignment algorithm (Dobin et al., 2013). Read normalization, reads per kilobase of transcript per million (RPKM), and differential gene expression were performed using the HOMER scripts analyzeRepeats.pl and getDiffExpression.pl with implementation of DESeq2 through R (Love et al., 2014). Heat maps of RPKM values for differentially expressed genes were generated with Cluster 3.0 (open source software by Michael Eisen) and visualized with Java TreeView (open source software by Alok J. Saldanha). The PANTHER pathway was used for GO analysis (Mi and Thomas, 2009). GSEA was used to compare gene expression changes detected upon TS or in Mi2 $\Delta$  relative to WT keratinocytes. Significantly up- and down-regulated genes (DESeq2- $\log_2$  fold change  $> 1$  or  $< -1$ , FDR  $< 0.05$ ) detected after TS were compared with all genes in the Mi2 $\Delta$  keratinocyte RNA-seq dataset using the preranked GSEA parameter for analysis. The all-genes Mi2 $\Delta$  keratinocyte RNA-seq dataset was ranked by  $\log_2$  fold change relative to the WT keratinocyte dataset.

### ATAC-seq and data analysis

$5 \times 10^4$  freshly sorted cells were used for ATAC-seq. The construction of cDNA libraries for ATAC-seq was performed as described (Buenrostro et al., 2013). Briefly, cells were subjected to transposition reaction with 3  $\mu$ l of the Tagment DNA enzyme at 37°C for 30 min (Nextera DNA sample preparation kit; Illumina). Transposed DNA was amplified and then purified using the Qiagen PCR Purification kit. The quality of libraries was tested by the Bioanalyzer (Agilent). Libraries were sequenced using a HiSeq 2000 platform at the Bauer Center Systems Biology Core at Harvard University. Read alignment was performed on the mm10 mouse assembly using the Bowtie2 genome alignment algorithm 1.4.1 with the sensitive option (Langmead et al., 2009). Duplicate reads were removed by Picard Tools (Broad Institute). Peak calling for ATAC-seq was performed with

MACS2 using the following parameters for peak calling: --keep-dup all --nomodel --shift 37 --extsize 73 (Zhang et al., 2008). Differentially enriched peaks in-between conditions were obtained by setting one condition as test and the other as input control.

### ChIP, ChIP-seq, and data analysis

ChIP was performed as previously described, with some modifications (Zhang et al., 2011; Hu et al., 2016). Cells were fixed with 1% fresh formaldehyde for 8 min at room temperature and then quenched by 2.5 M glycine. Cells were lysed in swelling buffer (25 mM Hepes-KOH at pH 7.8, 1.5 mM MgCl<sub>2</sub>, 10 mM KCl, 1% igepal, 1 mM 1,4-dithiothreitol, and 1 $\times$  protease inhibitor cocktail) for 10 min on ice, followed by Dounce homogenization. Nuclei were pelleted and resuspended in radioimmunoprecipitation assay buffer (10 mM Tris at pH 8.0, 140 mM NaCl, 1% Triton X-100, 0.1% Na-deoxycholate, 0.1% SDS, 1 mM EDTA, and 1 $\times$  protease inhibitor cocktail). Chromatin was sonicated to an average size of 300–500 bp with the Diagenode Bioruptor. Chromatin was cleared by centrifugation at 20,000 *g* for 10 min at 4°C followed by overnight incubation at 4°C with primary antibodies that were prebound to Dynabeads protein G (Life Technologies). The primary antibodies used were H3K27Ac (Abcam, ab4729), H3K4me3 (Active motif, 39159), RNApII (Abcam, ab817), c-JUN (Abcam, ab31419), JUNB (CST, C37F9), and Mi-2 $\beta$  (Abcam, ab72418; and CST, 12011). The number of cells used for each antibody in ChIP were  $\sim 2 \times 10^6$  cells for H3K27Ac,  $4 \times 10^6$  cells for H3K4me3 and RNApII,  $10^7$  cells for c-JUN,  $10^7$  cells for JUNB, and  $2 \times 10^7$  cells for Mi-2 $\beta$ . Chromatin was washed five times with immunoprecipitation wash buffer (10 mM Tris at pH 8.0, 500 mM NaCl, 1% Triton X-100, 0.1% Na-deoxycholate, and 0.1% SDS), followed by a wash with TE buffer (50 mM Tris at pH 8.0, 1 mM EDTA, and 50 mM NaCl). Chromatin was eluted and then de-crosslinked overnight at 65°C. DNA was purified using the DNA Clean and Concentration 5 kit (Zymo Research). Fold enrichment for ChIP-qPCR was calculated as the ratio of ratios obtained from Mi-2 $\beta$  ChIP and input control for Mi-2 $\beta$  target regulatory regions/negative control region. For ChIP-seq, the construction of cDNA libraries was performed as previously described (Hu et al., 2016). In brief, 2–50 ng of DNA was end-repaired, end-adenylated, and then ligated with Illumina TruSeq indexed adaptors. The ligated DNA was amplified, size-selected on a 2% agarose gel, and purified using a gel DNA recovery kit (Zymo Research). The libraries were sequenced using a HiSeq 2000 platform at the Bauer Center Systems Biology Core at Harvard University. Read alignment was performed on the hg19 assembly of the human genome using either Bowtie2 or the STAR genome mapper with the option to disable spliced alignments and prohibit gaps (Dobin et al., 2013). Peak calling for ChIP-seq was performed using the Homer findPeaks algorithm (Heinz et al., 2010). Differentially enriched peaks between two conditions were obtained by setting one condition as test and the other as input control. Heat maps of K-means clustering of ChIP-seq or ATAC-seq enriched peaks were generated using NGS.plot (Shen et al., 2014). Histograms of read densities for histone modifications and TFs at regulatory sites were plotted with NGS.plot (Shen et al., 2014). HOMER de novo motif discovery algorithm was used for motif

discovery analysis of TF and dATAC peaks. Venn diagrams were generated with the online-based Venny Tool.

### Co-immunoprecipitation analysis

Cells were lysed with lysis buffer (25 mM Tris at pH 7.5, 10% glycerol, 150 mM NaCl, 1.5 mM MgCl<sub>2</sub>, and protease inhibitors) containing 1% Triton X-100. The protein extracts were pre-cleared with Dynabeads protein G (Invitrogen). The pre-cleared extracts were incubated with the anti-Mi2β (Abcam, ab72418), JUNB (CST, C37F9), and cJUN (Abcam, ab31419) or the relevant isotype control in the presence of Dynabeads protein G and rotated overnight. Beads were then collected, washed at least five times with lysis buffer, and resuspended in SDS sample buffer. Eluents were subjected to SDS-PAGE and transferred to polyvinylidene difluoride membranes, probed with anti-Mi2β (CST, 12011), JUNB (CST, C37F9), cJUN (BD Bioscience, 610327), HDAC2 (CST, D6S5P), and MTA3 (Bethyl Laboratories, A300-160), and examined by autoradiography by Enhance Chemical Luminescence.

### Data availability

The sequencing datasets generated by this study have been deposited to National Center for Biotechnology Information and are accessible through Gene Expression Omnibus series accession no. GSE139685.

### Online supplemental material

Fig. S1 shows gene expression changes in mouse basal epidermis upon barrier disruption. Fig. S2 shows common transcription changes induced by barrier disruption and Mi-2β depletion in mouse basal epidermis. Fig. S3 shows changes in chromosome accessibility and associated transcriptional changes induced by barrier disruption and Mi-2β depletion in mouse basal epidermis. Fig. S4 provides evidence for a conserved Mi-2β-dependent mechanism of transcriptional regulation in mouse and human keratinocytes. Fig. S5 provides evidence for functional antagonism between AP1 complex and Mi-2β in human keratinocytes by changes in gene expression in single and double knockdown keratinocytes and by ChIP-seq analysis in these cells. Table S1 contains the datasets used to draw box-whisker plots in Fig. 1 E. Table S2 contains the IDs of genes that were commonly down-regulated by barrier disruption and Mi-2β depletion in mouse basal epidermis. Table S3 contains dATACi and dATACl peak files at 6 h after TS. Table S4 contains dATACi and dATACl peak files at 24 h after TS. Table S5 contains dATACi and dATACl peak files in Mi-2β-depleted compared with WT control keratinocytes. Table S6 contains Mi-2β ChIP-seq peaks identified in mouse keratinocytes. Table S7 contains Mi-2β ChIP-seq peaks in human keratinocytes. Table S8 contains cJUN and JUNB ChIP-seq peaks in human keratinocytes. Table S9 contains two datasets: one dataset of up-regulated genes upon Mi2KD in human keratinocytes and a second dataset of genes whose expression was reverted by concomitant knockdown of Mi-2β and c-JUN in human keratinocytes.

### Acknowledgments

We thank Drs. Rachael A. Clark and Jessica E. Teague and the Human Skin Disease Resource Center at Brigham and Women's

Hospital for providing us with discarded de-identified foreskin from human newborns. We thank Dr. Jin Mo Park for critical review of the manuscript, and Eleanor Wu and Robert Czyzewski for mouse husbandry.

Research was supported by National Institutes of Health grant R01AR069132 to K. Georgopoulos and M. Kashiwagi and by National Institutes of Health grant R21AR072976 to B.A. Morgan. K. Georgopoulos is a Massachusetts General Hospital scholar supported by Dr. Jean de Gunzburg. S. Shibata has been supported by fellowships from the Japanese Society for the Promotion of Science and Uehara Memorial Foundation. High-throughput RNA-seq was performed at the Bauer Center for Genomic Research at Harvard University and at Cutaneous Biology Research Center.

The authors declare no competing financial interests.

Author contributions: S. Shibata, M. Kashiwagi, K. Georgopoulos, and B.A. Morgan designed the experiments. S. Shibata and M. Kashiwagi performed the experiments. S. Shibata, M. Kashiwagi, and K. Georgopoulos analyzed the data. S. Shibata and K. Georgopoulos mainly wrote the manuscript. K. Georgopoulos and B.A. Morgan supervised the study.

Submitted: 31 December 2018

Revised: 29 July 2019

Accepted: 7 November 2019

### References

- Adhikary, G., J. Crish, J. Lass, and R.L. Eckert. 2004. Regulation of involucrin expression in normal human corneal epithelial cells: a role for activator protein one. *Invest. Ophthalmol. Vis. Sci.* 45:1080-1087. <https://doi.org/10.1167/iovs.03-1180>
- Aguilera, C., K. Nakagawa, R. Sancho, A. Chakraborty, B. Hendrich, and A. Behrens. 2011. c-Jun N-terminal phosphorylation antagonises recruitment of the Mbd3/NuRD repressor complex. *Nature*. 469:231-235. <https://doi.org/10.1038/nature09607>
- Becker, P.B. 2002. Nucleosome sliding: facts and fiction. *EMBO J.* 21: 4749-4753. <https://doi.org/10.1093/emboj/cdf486>
- Brehm, A., G. Längst, J. Kehle, C.R. Clapier, A. Imhof, A. Eberharter, J. Müller, and P.B. Becker. 2000. dMi-2 and ISWI chromatin remodelling factors have distinct nucleosome binding and mobilization properties. *EMBO J.* 19:4332-4341. <https://doi.org/10.1093/emboj/19.16.4332>
- Buenrostro, J.D., P.G. Giresi, L.C. Zaba, H.Y. Chang, and W.J. Greenleaf. 2013. Transposition of native chromatin for fast and sensitive epigenomic profiling of open chromatin, DNA-binding proteins and nucleosome position. *Nat. Methods*. 10:1213-1218. <https://doi.org/10.1038/nmeth.2688>
- Dainichi, T., A. Kitoh, A. Otsuka, S. Nakajima, T. Nomura, D.H. Kaplan, and K. Kabashima. 2018. The epithelial immune microenvironment (EIME) in atopic dermatitis and psoriasis. *Nat. Immunol.* 19:1286-1298. <https://doi.org/10.1038/s41590-018-0256-2>
- Dobin, A., C.A. Davis, F. Schlesinger, J. Drenkow, C. Zaleski, S. Jha, P. Batut, M. Chaisson, and T.R. Gingeras. 2013. STAR: ultrafast universal RNA-seq aligner. *Bioinformatics*. 29:15-21. <https://doi.org/10.1093/bioinformatics/bts635>
- Efimova, T., A.M. Broome, and R.L. Eckert. 2004. Protein kinase Cdelta regulates keratinocyte death and survival by regulating activity and subcellular localization of a p38δ-extracellular signal-regulated kinase 1/2 complex. *Mol. Cell. Biol.* 24:8167-8183. <https://doi.org/10.1128/MCB.24.18.8167-8183.2004>
- Ezhkova, E., H.A. Pasolli, J.S. Parker, N. Stokes, I.H. Su, G. Hannon, A. Tarakhovskiy, and E. Fuchs. 2009. Ezh2 orchestrates gene expression for the stepwise differentiation of tissue-specific stem cells. *Cell*. 136: 1122-1135. <https://doi.org/10.1016/j.cell.2008.12.043>
- Ge, Y., N.C. Gomez, R.C. Adam, M. Nikolova, H. Yang, A. Verma, C.P. Lu, L. Polak, S. Yuan, O. Elemento, and E. Fuchs. 2017. Stem cell lineage infidelity drives wound repair and cancer. *Cell*. 169:636-650.e14.

- Gnocchi, D., M. Pedrelli, E. Hurt-Camejo, and P. Parini. 2015. Lipids around the clock: focus on circadian rhythms and lipid metabolism. *Biology (Basel)*. 4:104–132.
- Gómez-Del Arco, P., E. Perdiguero, P.S. Yunes-Leites, R. Acín-Pérez, M. Zeini, A. García-Gomez, K. Sreenivasan, M. Jiménez-Alcázar, J. Segalés, D. López-Maderuelo, et al. 2016. The chromatin remodeling complex Chd4/NuRD controls striated muscle identity and metabolic homeostasis. *Cell Metab.* 23:881–892. <https://doi.org/10.1016/j.cmet.2016.04.008>
- Guinea-Viniegra, J., R. Zenz, H. Scheuch, D. Hnisz, M. Holcman, L. Bakiri, H.B. Schonthaler, M. Sibilia, and E.F. Wagner. 2009. TNF $\alpha$  shedding and epidermal inflammation are controlled by Jun proteins. *Genes Dev.* 23:2663–2674. <https://doi.org/10.1101/gad.543109>
- Heinz, S., C. Benner, N. Spann, E. Bertolino, Y.C. Lin, P. Laslo, J.X. Cheng, C. Murre, H. Singh, and C.K. Glass. 2010. Simple combinations of lineage-determining transcription factors prime cis-regulatory elements required for macrophage and B cell identities. *Mol. Cell.* 38:576–589. <https://doi.org/10.1016/j.molcel.2010.05.004>
- Hu, Y., Z. Zhang, M. Kashiwagi, T. Yoshida, I. Joshi, N. Jena, R. Somasundaram, A.O. Emmanuel, M. Sigvardsson, J. Fitamant, et al. 2016. Superenhancer reprogramming drives a B-cell-epithelial transition and high-risk leukemia. *Genes Dev.* 30:1971–1990. <https://doi.org/10.1101/gad.283762.116>
- Janich, P., K. Toufighi, G. Solanas, N.M. Luis, S. Minkwitz, L. Serrano, B. Lehner, and S.A. Benitah. 2013. Human epidermal stem cell function is regulated by circadian oscillations. *Cell Stem Cell.* 13:745–753. <https://doi.org/10.1016/j.stem.2013.09.004>
- Kashiwagi, M., B.A. Morgan, and K. Georgopoulos. 2007. The chromatin remodeler Mi-2 $\beta$  is required for establishment of the basal epidermis and normal differentiation of its progeny. *Development.* 134:1571–1582. <https://doi.org/10.1242/dev.001750>
- Kashiwagi, M., J. Hosoi, J.F. Lai, J. Brissette, S.F. Ziegler, B.A. Morgan, and K. Georgopoulos. 2017. Direct control of regulatory T cells by keratinocytes. *Nat. Immunol.* 18:334–343. <https://doi.org/10.1038/ni.3661>
- Keyes, B.E., S. Liu, A. Asare, S. Naik, J. Levorse, L. Polak, C.P. Lu, M. Nikolova, H.A. Pasolli, and E. Fuchs. 2016. Impaired epidermal to dendritic T cell signaling slows wound repair in aged skin. *Cell.* 167:1323–1338.e14.
- Kim, J., S. Sif, B. Jones, A. Jackson, J. Koipally, E. Heller, S. Winandy, A. Viel, A. Sawyer, T. Ikeda, et al. 1999. Ikaros DNA-binding proteins direct formation of chromatin remodeling complexes in lymphocytes. *Immunity.* 10:345–355. [https://doi.org/10.1016/S1074-7613\(00\)80034-5](https://doi.org/10.1016/S1074-7613(00)80034-5)
- Kolev, V., A. Mandinova, J. Guinea-Viniegra, B. Hu, K. Lefort, C. Lambertini, V. Neel, R. Dummer, E.F. Wagner, and G.P. Dotto. 2008. EGFR signalling as a negative regulator of Notch1 gene transcription and function in proliferating keratinocytes and cancer. *Nat. Cell Biol.* 10:902–911. <https://doi.org/10.1038/ncb1750>
- Lander, J.M., D.M. Supp, H. He, L.J. Martin, X. Chen, M.T. Weirauch, S.T. Boyce, and R. Kopan. 2017. Analysis of chromatin accessibility in human epidermis identifies putative barrier dysfunction-sensing enhancers. *PLoS One.* 12:e0184500. <https://doi.org/10.1371/journal.pone.0184500>
- Langmead, B., C. Trapnell, M. Pop, and S.L. Salzberg. 2009. Ultrafast and memory-efficient alignment of short DNA sequences to the human genome. *Genome Biol.* 10:R25. <https://doi.org/10.1186/gb-2009-10-3-r25>
- LeBoeuf, M., A. Terrell, S. Trivedi, S. Sinha, J.A. Epstein, E.N. Olson, E.E. Morrisey, and S.E. Millar. 2010. Hdac1 and Hdac2 act redundantly to control p63 and p53 functions in epidermal progenitor cells. *Dev. Cell.* 19:807–818. <https://doi.org/10.1016/j.devcel.2010.10.015>
- Love, M.I., W. Huber, and S. Anders. 2014. Moderated estimation of fold change and dispersion for RNA-seq data with DESeq2. *Genome Biol.* 15:550. <https://doi.org/10.1186/s13059-014-0550-8>
- Luo, J., F. Su, D. Chen, A. Shiloh, and W. Gu. 2000. Deacetylation of p53 modulates its effect on cell growth and apoptosis. *Nature.* 408:377–381. <https://doi.org/10.1038/35042612>
- Mehic, D., L. Bakiri, M. Ghannadan, E.F. Wagner, and E. Tschachler. 2005. Fos and jun proteins are specifically expressed during differentiation of human keratinocytes. *J. Invest. Dermatol.* 124:212–220. <https://doi.org/10.1111/j.0022-202X.2004.23558.x>
- Mi, H., and P. Thomas. 2009. PANTHER pathway: an ontology-based pathway database coupled with data analysis tools. *Methods Mol. Biol.* 563:123–140. [https://doi.org/10.1007/978-1-60761-175-2\\_7](https://doi.org/10.1007/978-1-60761-175-2_7)
- Nestle, F.O., P. Di Meglio, J.Z. Qin, and B.J. Nickoloff. 2009. Skin immune sentinels in health and disease. *Nat. Rev. Immunol.* 9:679–691. <https://doi.org/10.1038/nri2622>
- Pittelkow, M.R. 2005. Psoriasis: more than skin deep. *Nat. Med.* 11:17–18. <https://doi.org/10.1038/nm0105-17>
- Racila, D., M. Winter, M. Said, A. Tomanek-Chalkley, S. Wiechert, R.L. Eckert, and J.R. Bickenbach. 2011. Transient expression of OCT4 is sufficient to allow human keratinocytes to change their differentiation pathway. *Gene Ther.* 18:294–303. <https://doi.org/10.1038/gt.2010.148>
- Reynolds, N., P. Latos, A. Hynes-Allen, R. Loos, D. Leaford, A. O’Shaughnessy, O. Mosaku, J. Signolet, P. Brennecke, T. Kalkan, et al. 2012. NuRD suppresses pluripotency gene expression to promote transcriptional heterogeneity and lineage commitment. *Cell Stem Cell.* 10:583–594. <https://doi.org/10.1016/j.stem.2012.02.020>
- Risse, G., K. Jooss, M. Neuberger, H.J. Brüller, and R. Müller. 1989. Asymmetrical recognition of the palindromic API binding site (TRE) by Fos protein complexes. *EMBO J.* 8:3825–3832. <https://doi.org/10.1002/j.1460-2075.1989.tb08560.x>
- Rubin, A.J., B.C. Barajas, M. Furlan-Magaril, V. Lopez-Pajares, M.R. Mumbach, I. Howard, D.S. Kim, L.D. Boxer, J. Cairns, M. Spivakov, et al. 2017. Lineage-specific dynamic and pre-established enhancer-promoter contacts cooperate in terminal differentiation. *Nat. Genet.* 49:1522–1528. <https://doi.org/10.1038/ng.3935>
- Sano, S., K.S. Chan, S. Carbajal, J. Clifford, M. Peavey, K. Kiguchi, S. Itami, B.J. Nickoloff, and J. DiGiovanni. 2005. Stat3 links activated keratinocytes and immunocytes required for development of psoriasis in a novel transgenic mouse model. *Nat. Med.* 11:43–49. <https://doi.org/10.1038/nm1162>
- Segre, J.A. 2006. Epidermal barrier formation and recovery in skin disorders. *J. Clin. Invest.* 116:1150–1158. <https://doi.org/10.1172/JCI28521>
- Sextius, P., C. Marionnet, F.X. Bon, A.L. de La Chapelle, C. Tacheau, M. Lahfa, A. Mauviel, B.A. Bernard, J. Leclaire, F. Bernerd, and L. Dubertret. 2010. Large scale study of epidermal recovery after stratum corneum removal: dynamics of genomic response. *Exp. Dermatol.* 19:259–268. <https://doi.org/10.1111/j.1600-0625.2009.00976.x>
- Shaulian, E., and M. Karin. 2002. AP-1 as a regulator of cell life and death. *Nat. Cell Biol.* 4:E131–E136. <https://doi.org/10.1038/ncb0502-e131>
- Shen, L., N. Shao, X. Liu, and E. Nestler. 2014. ngs.plot: Quick mining and visualization of next-generation sequencing data by integrating genomic databases. *BMC Genomics.* 15:284. <https://doi.org/10.1186/1471-2164-15-284>
- Takahashi, H., M. Ibe, S. Nakamura, A. Ishida-Yamamoto, Y. Hashimoto, and H. Iizuka. 2002. Extracellular regulated kinase and c-jun N-terminal kinase are activated in psoriatic involved epidermis. *J. Dermatol. Sci.* 30:94–99. [https://doi.org/10.1016/S0923-1811\(02\)00664-6](https://doi.org/10.1016/S0923-1811(02)00664-6)
- Tong, J.K., C.A. Hassig, G.R. Schnitzler, R.E. Kingston, and S.L. Schreiber. 1998. Chromatin deacetylation by an ATP-dependent nucleosome remodeling complex. *Nature.* 395:917–921. <https://doi.org/10.1038/27699>
- Welter, J.F., and R.L. Eckert. 1995. Differential expression of the fos and jun family members c-fos, fosB, Fra-1, Fra-2, c-jun, junB and junD during human epidermal keratinocyte differentiation. *Oncogene.* 11:2681–2687.
- Williams, C.J., T. Naito, P.G. Arco, J.R. Seavitt, S.M. Cashman, B. De Souza, X. Qi, P. Keables, U.H. Von Andrian, and K. Georgopoulos. 2004. The chromatin remodeler Mi-2 $\beta$  is required for CD4 expression and T cell development. *Immunity.* 20:719–733. <https://doi.org/10.1016/j.immuni.2004.05.005>
- Wurm, S., J. Zhang, J. Guinea-Viniegra, F. García, J. Muñoz, L. Bakiri, E. Ezhkova, and E.F. Wagner. 2015. Terminal epidermal differentiation is regulated by the interaction of Fra-2/AP-1 with Ezh2 and ERK1/2. *Genes Dev.* 29:144–156. <https://doi.org/10.1101/gad.249748.114>
- Xue, Y., J. Wong, G.T. Moreno, M.K. Young, J. Côté, and W. Wang. 1998. NURD, a novel complex with both ATP-dependent chromatin-remodeling and histone deacetylase activities. *Mol. Cell.* 2:851–861. [https://doi.org/10.1016/S1097-2765\(00\)80299-3](https://doi.org/10.1016/S1097-2765(00)80299-3)
- Yamada, T., Y. Yang, M. Hemberg, T. Yoshida, H.Y. Cho, J.P. Murphy, D. Fioravante, W.G. Regehr, S.P. Gygi, K. Georgopoulos, and A. Bonni. 2014. Promoter decommissioning by the NuRD chromatin remodeling complex triggers synaptic connectivity in the mammalian brain. *Neuron.* 83:122–134. <https://doi.org/10.1016/j.neuron.2014.05.039>
- Yoshida, T., I. Hazan, J. Zhang, S.Y. Ng, T. Naito, H.J. Snippert, E.J. Heller, X. Qi, L.N. Lawton, C.J. Williams, and K. Georgopoulos. 2008. The role of the chromatin remodeler Mi-2 $\beta$  in hematopoietic stem cell self-renewal and multilineage differentiation. *Genes Dev.* 22:1174–1189. <https://doi.org/10.1101/gad.1642808>
- Yoshida, T., Y. Hu, Z. Zhang, A.O. Emmanuel, K. Galani, B. Muhire, H.J. Snippert, C.J. Williams, M.Y. Tolstourkov, F. Gounari, and K. Georgopoulos. 2019. Chromatin restriction by the nucleosome remodeler Mi-2 $\beta$  and functional interplay with lineage-specific transcription regulators control B-cell differentiation. *Genes Dev.* 33:763–781. <https://doi.org/10.1101/gad.321901.118>

- Zenz, R., R. Eferl, L. Kenner, L. Florin, L. Hummerich, D. Mehic, H. Scheuch, P. Angel, E. Tschachler, and E.F. Wagner. 2005. Psoriasis-like skin disease and arthritis caused by inducible epidermal deletion of Jun proteins. *Nature*. 437:369–375. <https://doi.org/10.1038/nature03963>
- Zhang, Y., G. LeRoy, H.P. Seelig, W.S. Lane, and D. Reinberg. 1998. The dermatomyositis-specific autoantigen Mi2 is a component of a complex containing histone deacetylase and nucleosome remodeling activities. *Cell*. 95:279–289. [https://doi.org/10.1016/S0092-8674\(00\)81758-4](https://doi.org/10.1016/S0092-8674(00)81758-4)
- Zhang, Y., T. Liu, C.A. Meyer, J. Eeckhoute, D.S. Johnson, B.E. Bernstein, C. Nusbaum, R.M. Myers, M. Brown, W. Li, and X.S. Liu. 2008. Model-based analysis of ChIP-Seq (MACS). *Genome Biol.* 9:R137. <https://doi.org/10.1186/gb-2008-9-9-r137>
- Zhang, J., A.F. Jackson, T. Naito, M. Dose, J. Seavitt, F. Liu, E.J. Heller, M. Kashiwagi, T. Yoshida, F. Gounari, et al. 2011. Harnessing of the nucleosome-remodeling-deacetylase complex controls lymphocyte development and prevents leukemogenesis. *Nat. Immunol.* 13:86–94. <https://doi.org/10.1038/ni.2150>

## Supplemental material

Shibata et al., <https://doi.org/10.1084/jem.20182402>

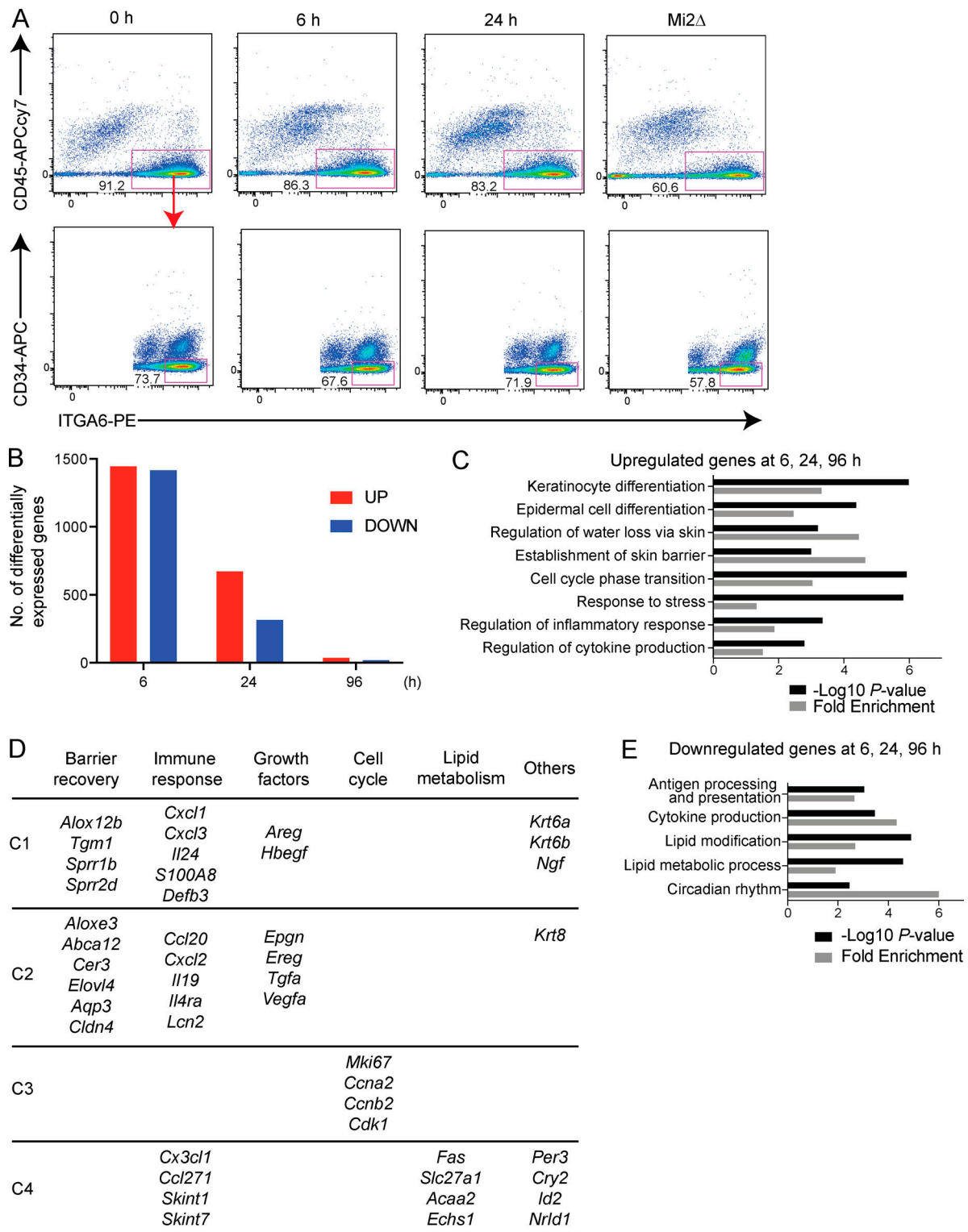


Figure S1. **Sorting basal keratinocytes after skin barrier disruption and profiling changes in gene expression.** (A) Sorting strategy for keratinocytes obtained from epidermis before (0 h) and after TS (6 or 24 h) or after Mi-2 $\beta$  depletion (Mi2 $\Delta$ ). After doublet exclusion (forward scatter–area versus forward scatter–height), cells were gated for size and sorted for ITGA6<sup>mid-to-high</sup> CD45<sup>-</sup> CD34<sup>-</sup> expression. (B) Number of differentially expressed genes at 6–96 h after barrier disruption. (C) Pathway analysis of all significantly up-regulated genes ( $\log_2$  fold change >1, FDR <0.05) detected at 6, 24, and 96 h after TS is shown. Select GO pathways and associated P values ( $-\log_{10}$ ) with fold enrichment are provided. (D) Representative genes in the clusters (C1, C2, C3, and C4) of the heatmap shown in Fig. 1 E, with their functional categories, are listed. (E) Pathway analysis of all significantly down-regulated genes ( $\log_2$  fold change >1, FDR <0.05) at 6, 24, and 96 h after TS is shown. Select GO pathways and associated P values ( $-\log_{10}$ ) with fold enrichment are provided. Sorting data shown in A are representative of >10 experiments performed with 2 pooled mouse skin samples for each experimental point (i.e., 0, 6, and 24 h) and Mi2 $\Delta$ . RNA-seq studies (B–E) were performed with biological replicates described in Fig. 1.

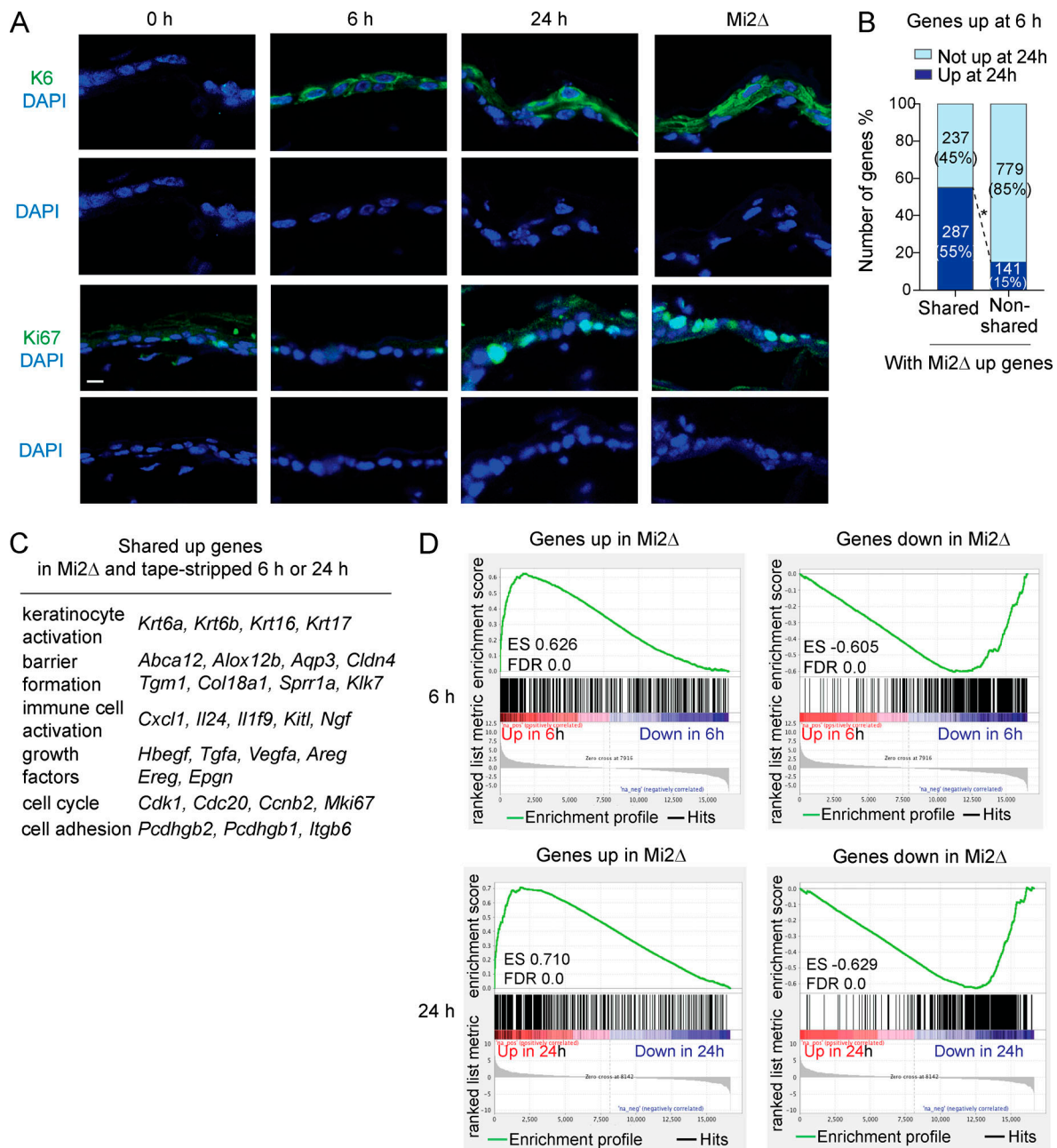


Figure S2. **Comparative analysis of histological and transcriptional responses induced by barrier disruption and Mi-2β depletion.** (A) Expression of K6 (green) and Ki67 (green) proteins by immunofluorescence at 0 h and in tape-stripped (6 and 24 h) and Mi2Δ epidermis. Nuclei were visualized by counterstaining with DAPI (blue). Scale bar = 10 μm. (B) The percentage of genes that were significantly up-regulated at 6 h and that still displayed a significant increase at 24 h after TS (dark blue) is shown as bar graphs on the left. The number and percentage of genes in the two categories of shared or nonshared genes distinguished by their significant up-regulation or not in Mi2Δ keratinocytes are also shown. (C) Select genes from 287 shared gene targets between Mi2Δ keratinocytes and tape-stripped keratinocytes at 6 or 24 h are shown together with their functional ontology. (D) GSEA comparing significantly up- or down-regulated genes in Mi2Δ keratinocytes with the transcriptional profiles of tape-stripped keratinocytes (6 h: top; 24 h: bottom). The enrichment profile is plotted, and calculated ES and FDR are provided. Histological images shown in A are representative of two independent experiments with a total of three mice per group. RNA-seq studies in B–D were performed with biological replicates described in Fig. 1.



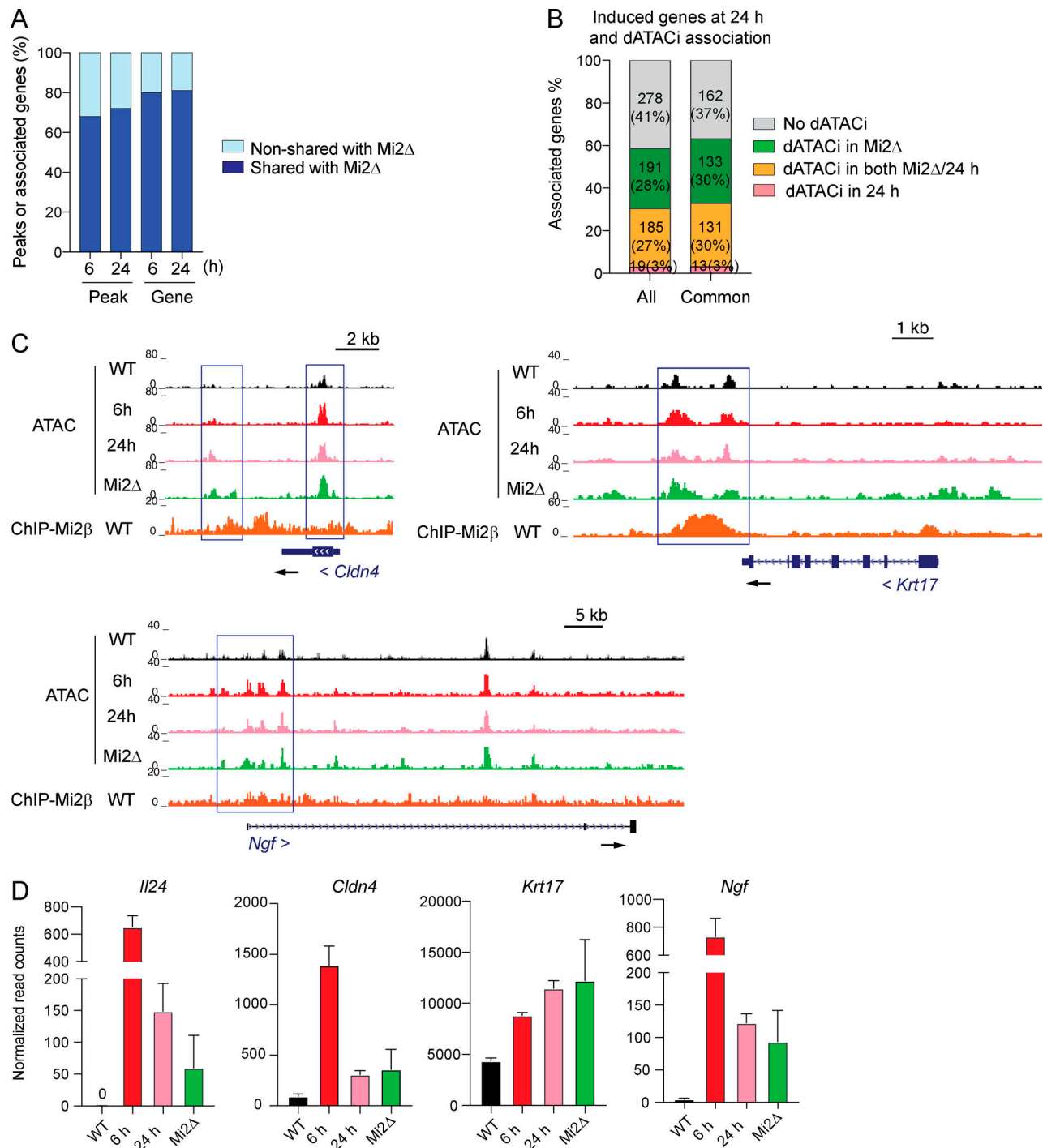


Figure S3. **Comparative analysis of changes in chromatin accessibility and associated transcriptional output induced by barrier disruption and/or Mi-2β depletion.** (A) The frequency of peak overlap between dATACi peaks detected in tape-stripped (6 or 24 h) keratinocytes and Mi2Δ keratinocytes is shown on the left. The overlap of genes associated with these dATACi peaks is shown on the right. (B) The frequency and number of significantly up-regulated genes ( $|\log_2$  fold change  $\geq 1$ , FDR  $< 0.05$ ) after 24 h of TS that were associated with dATACi peaks at the same time point or/and with dATACi peaks in Mi2Δ keratinocytes are shown on the left (All). Genes with dATACi peak association under one (Mi2Δ: green; 24 h: pink), both (orange), or no (gray) conditions are color coded. A similar presentation is shown on the right for genes that were commonly up-regulated at 24 h after TS and in Mi2Δ keratinocytes (Common). (C) Genome browser tracks of normalized ATAC-seq reads across the *Cldn4*, *Krt17*, and *Ngf* locus, showing increased chromatin accessibility (ATAC-seq) after TS (6 or 24 h) or in Mi2Δ keratinocytes. Mi-2β ChIP-seq in mouse primary cultured keratinocytes is also shown. Shared dATACi peaks are outlined with a blue rectangle. (D) Expression of *Il24*, *Cldn4*, *Krt17*, and *Ngf* (normalized read counts from RNA-seq) is shown for WT, tape-stripped (6 or 24 h), and Mi2Δ keratinocytes as bar graphs with mean and SEM. ATAC-seq and RNA-seq studies were performed as described in Figs. 1 and 3.

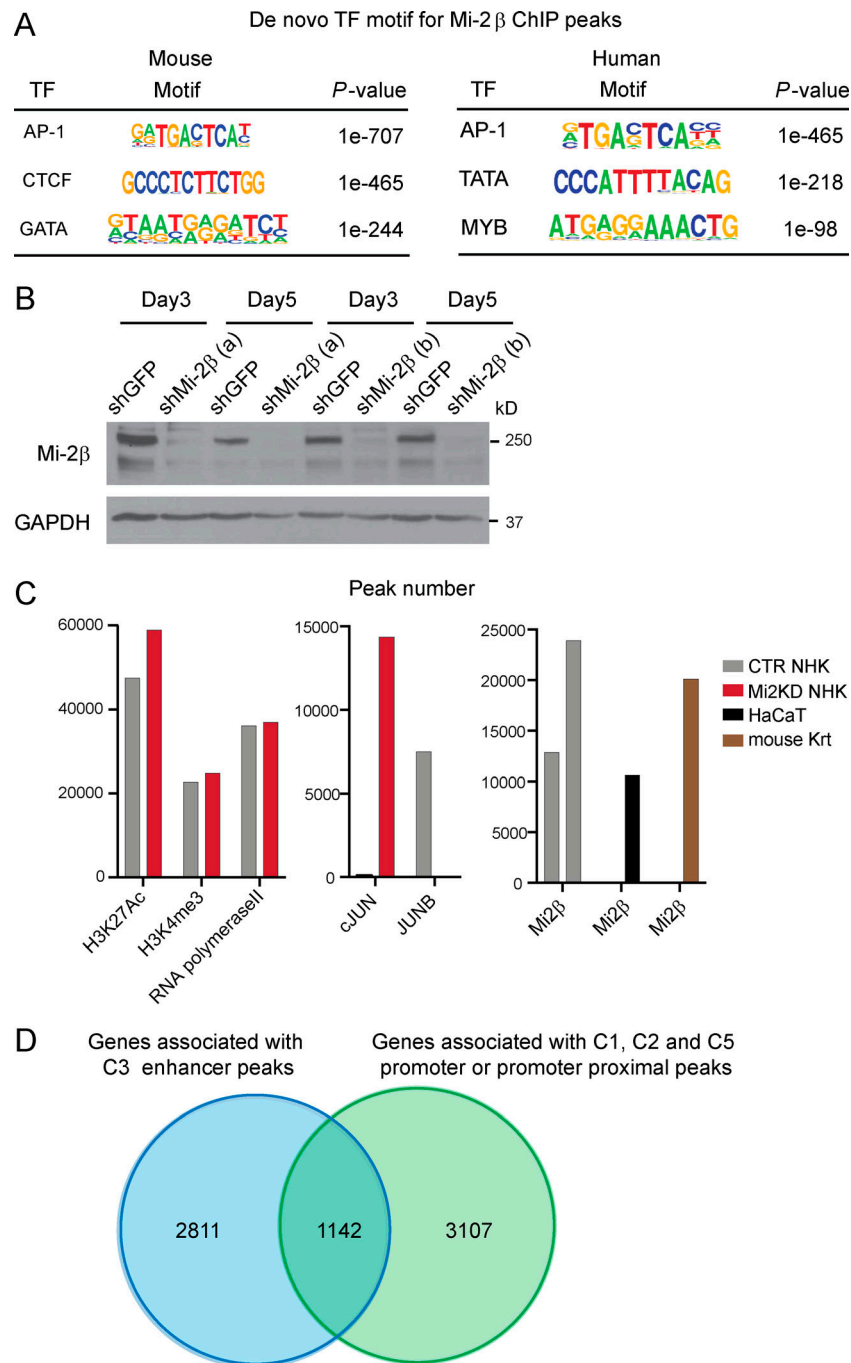
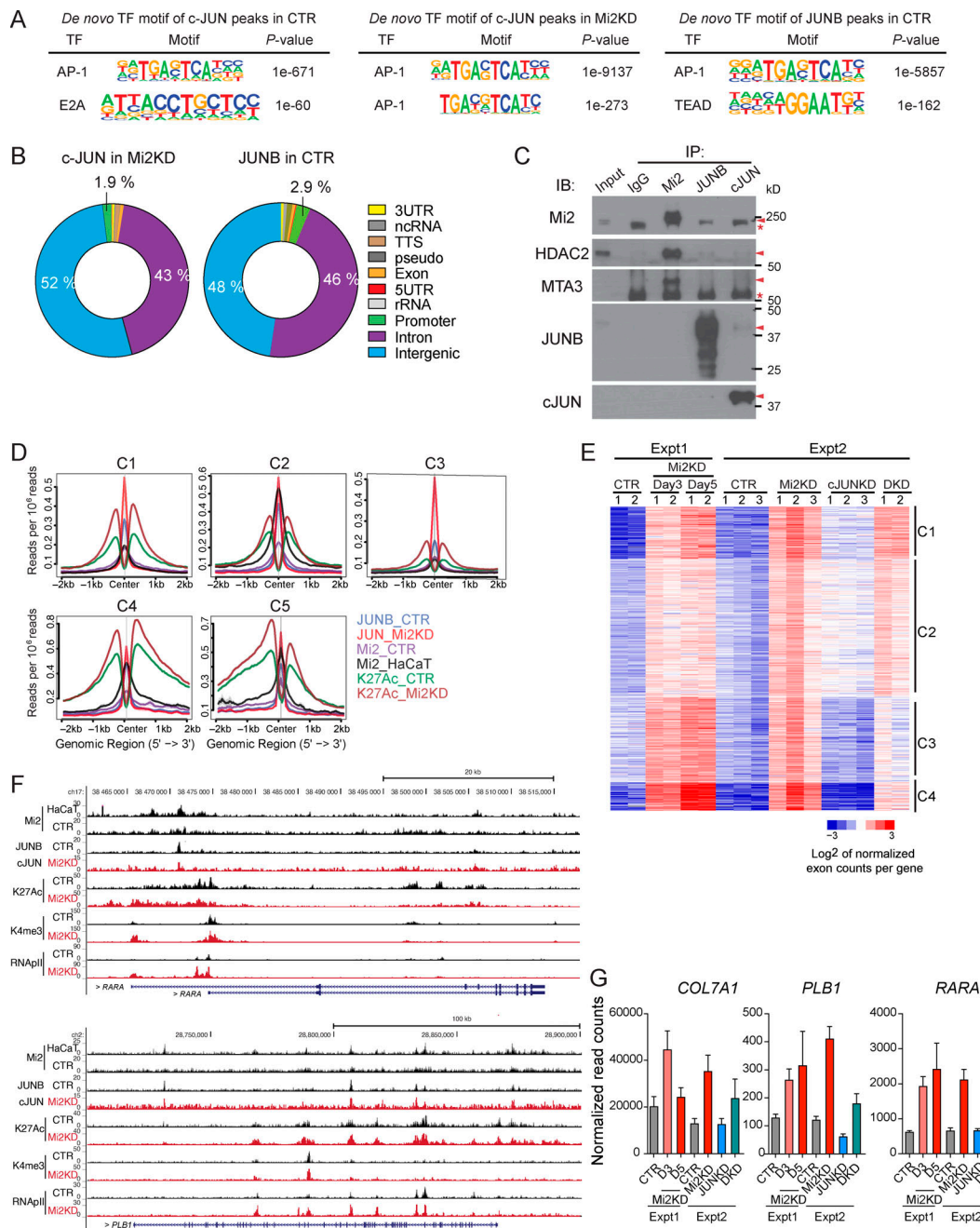


Figure S4. **Epigenetic landscape, transcription factors, and genes associated with Mi-2β chromatin enriched peaks in mouse and human keratinocytes.** (A) De novo motif discovery with P values for potential TF binding at Mi-2β peaks in mouse and human keratinocytes. (B) Immunoblotting for Mi-2β at days 3 and 5 after Mi-2β shRNA lentiviral transduction in NHKs showing efficient Mi-2β depletion. Data from two different shRNA experiments are shown. (C) Peak analysis for H3K27Ac, H3K4me3, RNAPII, JUN, JUNB, and Mi-2β ChIP-seq datasets is provided for CTR (gray) and Mi2KD (red) NHKs, HaCaTs (black), and mouse primary cultured keratinocytes (Krt; brown). (D) Overlap between genes associated with Mi-2β-bound promoter and promoter-proximal regions (C1, C2, and C5) and Mi-2β-bound enhancers (C3) as shown in Fig. 5 F. ChIP-seq studies were performed as described in Fig. 5. Immunoblot data shown in B are representative of >10 independent experiments.



**Figure S5. Analysis of c-JUN and JUNB chromatin enrichment in keratinocytes and study of functional antagonism of c-JUN and Mi-2β.** (A) *De novo* motif discovery for TF binding sites associated with c-JUN peaks in CTR and Mi2KD human primary keratinocytes and JUNB peaks in CTR human primary keratinocytes. (B) Genomic annotation of c-JUN peaks in Mi2KD human primary keratinocytes and JUNB peaks in CTR human primary keratinocytes represented by color shading of respective genomic locations as shown on the right. ncRNA, noncoding RNA; TTS, transcriptional termination sites. (C) Co-immunoprecipitation analysis with Mi-2β, JUNB, and cJUN in human primary keratinocytes. Protein extracts from human primary keratinocytes were immunoprecipitated with anti-Mi-2β, JUNB, and cJUN and analyzed by immunoblotting (IB) with antibodies against Mi-2β, HDAC2, MTA3, JUNB, and cJUN. Input (3% of total lysate) and IP with normal rabbit IgG were used as controls. Arrowheads indicate the relevant protein bands. Stars indicate the irrelevant bands. IP, immunoprecipitations. (D) Occupancy of TFs (JUNB, JUN, and Mi-2β) and H3K27Ac at c-JUN peak clusters C1–C5 as shown in the heatmap of Fig. 6 F. Read density (read count per million mapped reads) obtained from ChIP-seq datasets centered at c-JUN peaks (±2 kb) in Mi2KD human primary keratinocytes is shown. (E) Heatmap of K-means clustering analysis of differentially expressed genes (1,611) in Mi2KD compared with primary NHKs as determined by DESeq2 before and at days 3–5 after Mi2KD. Normalized expression of these genes is shown in CTR, Mi2KD, cJUNKD, and DKD human primary keratinocytes. Induced expression in clusters C2–C4 was reduced in the DKD, whereas expression in C1 was unaffected. Data from two different experiments (Expt), each with two replicates were used in this analysis. (F) Genome browser tracks of normalized ChIP-seq reads for TFs (JUNB, JUN, Mi-2β, and RNAPII) and histone modifications (H3K27Ac and H3K4me3) generated from NHKs (CTR, black histogram), Mi2KD NHKs (red histogram), and HaCaT cells (black histogram) are shown at the *RARA* and *PLB1* locus. (G) Expression of *COL7A1*, *RARA*, and *PLB1* (normalized read counts from RNA-seq) is shown for CTR, Mi2KD, cJUNKD, and DKD. ChIP-seq and RNA-seq studies were performed as described in Figs. 5 and 7. Co-immunoprecipitation data shown in C are representative of three independent experiments.

Tables S1–S9 are provided online as separate Excel files. Table S1 contains the datasets used to draw box-whisker plots in Fig. 1 E. Table S2 contains the IDs of genes that were commonly de-regulated by barrier disruption and Mi-2 $\beta$  depletion in mouse basal epidermis. Table S3 contains dATACi and dATACl peak files at 6 h after TS. Table S4 contains dATACi and dATACl peak files at 24 h after TS. Table S5 contains dATACi and dATACl peak files in Mi-2 $\beta$ -depleted compared with WT control keratinocytes. Table S6 contains Mi-2 $\beta$  ChIP-seq peaks identified in mouse keratinocytes. Table S7 contains Mi-2 $\beta$  ChIP-seq peaks in human keratinocytes. Table S8 contains cJUN and JUNB ChIP-seq peaks in human keratinocytes. Table S9 contains two datasets: one dataset of up-regulated genes upon Mi2KD in human keratinocytes and a second dataset of genes whose expression was reverted by concomitant knockdown of Mi-2 $\beta$  and c-JUN in human keratinocytes.